Study of neutrino-nucleus reactions with CRISP model ($0 < E_\nu < 3$ GeV)

R. Perez [*] and A. Deppman [†]
Instituto de Física da Universidade de São Paulo-IFUSP Rua do Matáo, Travessa R, 187, São Paulo, 05508-090, Brasil

A. R. Samana, Evandro Andrade-II, and F. G. Velasco
Universidade Estadual de Santa Cruz—UESC, Rodovia Jorge Amado km 16, Ilhéus, 45662-900, Brasil

F. Guzmán
Instituto Superior de Tecnologías y Ciencias Aplicadas—InSTEC, Avenida Salvador Allende esquina Luaces, La Habana, 10400, Cuba

(Received 25 June 2021; revised 26 October 2021; accepted 18 February 2022; published 22 March 2022)

The neutrino-nucleus reactions are studied at energies from 0 to 3 GeV, using the CRISP program. To simulate these reactions, CRISP uses the Monte Carlo method through an intranuclear cascade model. Quasielastic, baryonic resonance formation, and deep inelastic scattering channels for the neutrino-nucleon interaction are considered. The total and differential particle emission cross sections were obtained, resulting in a good agreement with the values reported by the MiniBooNE experiment. The influence of nuclear effects on the studied reactions, such as fermionic motion and the Pauli blocking mechanism, was shown. By using only neutrino-nucleon interactions (1p1h), it was necessary to modify the axial mass of the quasielastic channels to $M_A = 1.35$ GeV (much higher than the value obtained in neutrino-deuterium reactions, $M_A = 1.026$ GeV). The problem in adjusting M_A is the need for known $M_A(A)$, where A is the mass number, in case we want to study another target nucleus. The introduction of the 2p2h processes solves this and also reproduces the experimental data with $M_A = 1.026$ GeV. To show this, we use the transverse enhancement model to implement the 2p2h dynamic in CRISP, in such a way that it can be used with any target nucleus.

DOI: 10.1103/PhysRevD.105.063016

I. INTRODUCTION

The neutrino appears today as one of the most intriguing elementary particles of the Standard Model [1]. Its low mass identified by means of the so-called neutrino oscillation [2] confers to the particle unique properties. However, its weak interaction with matter [3,4] poses serious challenges to the investigation of the particle's properties. Several experiments were developed to investigate the neutrinos properties, as MiniBooNE [5], SciBooNE [6], MINERvA [7], T2K [8], MINOS [9], and NOνA [10], and new experiments are under development, such as ANNIE [11], DUNE [12], and Hyper-Kamiokande [13].

Neutrinos can interact with the nuclei by coherent [14–16] and incoherent [1,17–20] mechanisms. In the coherent form, the neutrino interacts with the nucleus as a whole, and in the incoherent form, the neutrino interacts with the components of the nucleus separately, that is, with protons and neutrons.

In this work, we investigate the neutrino-nucleus interaction using a Monte Carlo approach. The neutrino-nucleon interaction is studied utilizing the (quasi)elastic, baryon resonance production, and deep inelastic scattering (DIS) channels. For each of these channels, the charged current (CC) and neutral current (NC) interactions are considered. In addition to the neutrino-nucleon interaction, the importance of interaction processes with more than one nucleon at a time (2p2h, for example) for the charged current quasielastic channel (CCQE) is studied. The nuclear effects taken into account include the anticommutation of the fermionic states, the modifications of the nuclear density during the time evolution of the reaction, the thermalization of the nucleus, the formation and decay of baryonic resonances, and the preequilibrium emission.

Computing the neutrino-nucleon reactions is necessary to introduce some nucleon form factors [1,21]. These form factors are functions to adapt the elementary neutrino-quark to the neutrino-nucleon interaction. For example, in CCQE and neutral current elastic (NCE) channels, a set of form factors frequently used in the literature is the vector $F^V_{1,2}$, axial F_A, pseudoscalar F_P, and strangeness F_S form

[*] rvarona90@gmail.com
[†] deppman@usp.br

factors. Using the conserved vector current hypothesis [22,23], $F^V_{1,2}$ can be related to the Sachs form factors [24], which are well known and studied from the electromagnetic electron-nucleon interaction [25]. Similarly, F_P can be related to F_A by the partially conserved axial current hypothesis [23]. Thus, F_S and F_A are left free and have to be parametrized. These form factors are exclusively dependent on the neutrino-nucleon interaction.

For an appropriate determination of the form factors, it is necessary to have neutrino-nucleus measurements in the most exclusive way possible. Ideally, measurements of CCQE and NCE channels should be made separately. The CCQE channel depends only on F_A and therefore can be used to determine this form factor. On the other hand, the NCE channel depends on both F_A and F_S, and with F_A determined from the CCQE channel, it is possible to compute F_S.

Because of the low neutrino-matter cross section, there is extra difficulty in setting up the experiments. Until now, we have scarce measurement data from the CCQE and NCE channels for the neutrino-nucleus reactions [5,7,26,27]. This point is where Monte Carlo simulations become helpful. First, they are an excellent tool for comparing theoretical models with experimental data and making the corresponding parameter fits. Second, they serve to obtain theoretical results for reactions where experimental data are not available, which can be extremely important in the preparation of future experiments.

The CRISP model [28] is a useful tool to investigate several properties of nuclear reactions. It uses Monte Carlo and quantum dynamics methods to provide reliable predictions on several aspects of the reaction process. The model can be divided into three steps: the primary interaction, the intranuclear process, and the residual nucleus decay by spallation or fission.

The primary reaction describes the initial interaction of the incident particle with the proton and the neutron in the vacuum. In the CRISP model, we can accurately describe the reactions induced by photons [28–30], electrons [31,32], protons [33,34], and light nuclei [35,36], and in this work, we continue the neutrino induced reaction [37]. The model can also be used to study ultraperipheral high-energy collisions and production and decay of strange particles. Most of the results presented in this work are derived from this step, so we postpone a more detailed description to the next sections.

The second step, the intranuclear cascade, represents one of the most advanced aspects of the model. It includes a realistic description of the nuclear dynamics before and after the primary interaction, taking into consideration many of the most important nuclear processes that occur in this step of the reaction. Protons and neutrons are described as Fermi gases contained by the nuclear potential, with the restriction that a shell structure with well-defined occupation numbers is assumed. During the time evolution of the cascade, each energy cell does not allow more nucleons than its occupancy number, which determines in a deterministic way the inclusion of the Pauli blocking mechanism. In the ground state, only the lowest levels are occupied. After the primary interaction, the movements of all particles in the compound system are considered, which allows a reliable description of the local modifications of the nuclear density due to the momentum transferred to the nucleons by the intranuclear cascade dynamics. The accurate evaluation of the Pauli exclusion principle at every step of the dynamic confers to the model a unique characteristic that allows the precise reproduction of the dynamical evolution of the system without the need of artificial parameters to regulate the outcomes of the reaction. This aspect makes the CRISP model a trustworthy method to predict the results of nuclear reactions even where no experiments are available to anchor the theoretical calculations. The intranuclear cascade process starts as soon as the primary interaction products are created. The cascade continues until the residual nucleus is completely thermalized. Therefore, preequilibrium emissions are completely considered in the standard way. The production of nucleons, mesons, and clusters, like deuterons, are considered in this step.

With thermalization, the residual nucleus starts the decaying process, with the emission of nucleons (spallation process) or fission. This process continues until the excitation energy of the residual nucleus is exhausted. In the case of fission, symmetric and asymmetric fission fragments can be generated. Since in the present work this part of the model is less relevant, we address the interested reader to Refs. [29,38].

Before going into the details of the work described here, we would like to point out some of the main contributions we consider this work brings to the field. The first one is to offer an additional tool for studying the neutrino-nucleus interaction with the inclusion of this mechanism of reaction in the CRISP model. This model has been extensively tested for many nuclei with masses in the range $12 < A < 240$, for reactions induced by photons, protons, electrons, and light nuclei in the energy range from $50\ \mathrm{MeV} < E < 4\ \mathrm{TeV}$. For allowing the realistic description of the important aspects of nuclear structure involved in the reactions, the CRISP model is equipped with a default square-well nuclear potential, which gives good results for larger nuclei, and with a harmonic nuclear potential, which is necessary for light nuclei.

The CRISP allows us to study several aspects of nuclear reactions, with different observables and reaction channels being described. One of the main aspects of the model is the use of realistic models of the nuclear mechanisms with an emphasis in the reduction of the number of adjustable parameters. At all stages of the calculations, the relativistic dynamics is considered. Also, the parameters are global, in the sense that they are not adjusted for specific reactions or channels but describe the whole nuclear dynamics during the reaction. With this line of development, the reliability of the model for searching for new phenomena where no data are available is reinforced.

Specifically, for the neutrino-nucleus interaction we give, aside from the new tool, there are some interesting studies regarding points that might still be unclear in the field. We anticipate a few of them here:

(1) For the CCQE channel, we used two approaches: a) We used an axial mass of 1.35 GeV without 2p2h states, in order to compare with the well-known NUANCE model, which uses also a relativistic Fermi gas model but adopts *ad hoc* parameters for the Pauli blocking mechanism. Here, our main improvement regards the consideration of the Pauli blocking in a strict way, an aspect that Ref. [28] showed to be fundamental to correctly describe the fast stage of the nuclear reaction. b) Then, we included the 2p2h states and observed that the available data can be reproduced with an axial mass 1.026 GeV, which is in accordance with the expected axial mass [39]. Although this is already a known result, we show that the CRISP model reproduces the effects expected and also offers additional possibilities to investigate the two mechanisms by searching for different outcomes of the nuclear reaction process. The best-known models on neutrino-nucleus interaction provide only energy and angular momentum distribution, while the CRISP model allows investigating many other aspects of the reaction, e.g., correlations in multiparticle emission, different reaction channels, and coupling with more complex nuclear states. In the specific case of the 2p2h mechanism, the CRISP model allows investigating the correlation of the pair of nucleons in the final states after considering its propagation inside the nucleus.

(2) For the NCE channel, the experimental cross section of transferred momentum shows a peak for $Q^2 \approx 0.2\ \mathrm{GeV}^2$. This peak, associated with the Pauli blocking mechanism, cannot be reproduced by CRISP. In this work, we showed how with intranuclear cascade dynamics and a relativistic Fermi gas (RFG) model the reproduction of this peak should not be expected. To obtain the peak, NUANCE needs to modify the neutrino-nucleon cross section through a multiplicative factor. It is important to note that the experimental cross section depends on this factor since NUANCE was used in the unfolding process of the MiniBooNE experiment [40].

II. CRISP MODEL

The CRISP model is a computational program wrote in C++ with the objective of simulating nuclear reactions. The typical situation to use the CRISP is the following: we have an incident particle with energy T and a target nuclei in rest. To simulate this, the CRISP divides the reaction in three fundamental steps: the primary interaction, the intranuclear cascade, and the evaporation-fission competition. A more complete description of these phases, for the specific case of neutrino-nucleus reaction, is presented below.

A. Primary interaction

The primary interaction or the event generation phase introduces the initial conditions into the CRISP, puts the incident neutrino into the target nuclei, and runs the first neutrino-nucleon interaction. The initial conditions are an incident neutrino with energy T and a target nucleus at rest in the center of a Cartesian coordinate system. The neutrino moves in the direction of the nucleus and parallel to the z axis of the coordinate system. The initial "x" and "y" coordinates of the neutrino in the nuclear surface are aleatory randomized, using a uniform probabilistic density function in the circle $x^2 + y^2 \leq R^2$, where R is the nuclear radius. The z coordinate is calculated as $z = -\sqrt{x^2 + y^2}$.

The target nucleus consists of a (global) RFG in which protons and neutrons are subjected to a spherical nuclear potential of depth $V_0 = E_f + B$. Here, E_f is the Fermi energy, and $B = 8$ MeV is the nucleon separation energy. The target has a shell structure in the momentum space with a well-determined occupation number of each level. The nth level is characterized by the integers quantum numbers n, n_x, n_y, and n_z, which must satisfy the condition [28]

$$n_x^2 + n_y^2 + n_z^2 = n^2. \tag{1}$$

The number of combinations of n_x, n_y, and n_z that satisfy Eq. (1) determines the number of possible states for each n. Because of the spin and isospin degrees of freedom, each state can be occupied up to four nucleons. We apply an additional restriction: the first level can be occupied by up to two protons and two neutrons, which is consistent with the nuclear shell model derived from a Wood-Saxon potential. The layer momentum gap Δp can be determined with the Fermi's momentum and the number of layers until the Fermi level. The relation between nucleon momentum and its quantum numbers is

$$p^2 = p_x^2 + p_y^2 + p_z^2 = (n_x^2 + n_y^2 + n_z^2)(\Delta p)^2 = n^2(\Delta p)^2. \tag{2}$$

The nucleon momentum and the occupation number of each level are helpful for the implementation of the Pauli principle. Therefore, an energy level with more particles than its occupation number is not allowed.

Initially, the target nucleus is in its ground state, with the nucleons occupying the lowest energy levels. The condition of a minimal energy state implies that nucleons are in the inferior momentum surface of each momentum layer. Those initial conditions are essential to eliminate non-physical effects observed in other generators. The most important one is the spontaneous nucleon emission, which is impossible in our model because there are not physically accessible states under our ground-state configuration.

Kinematically, all particles move in a linear and uniform motion into the studied nucleus. When two particles reach their minimal distance, $b_{\min}$, the possibility of interaction between them is considered. For the initial neutrino-nucleon interaction, the following conditions are necessary: (i) The total neutrino-nucleon cross section, $\sigma_{\nu-N_i}$, must be larger than the geometrical cross section $\pi b_{\min}^2$. (2) The Pauli blocking mechanism must allow the final particle configuration.

When any of the above conditions are not met, then the event generator is reset, and this simulation is counted as an attempted cascade. Otherwise, the event generator is stopped, and subsequently, the intranuclear cascade phase is started.

B. Intranuclear cascade

The intranuclear cascade consists of executing all the possible time-ordered interactions inside the nucleus. In this step, similarly to the event generator, the particles have a linear and uniform motion. Three kinds of interactions are considered: the particle-particle collision, the particle decay, and the particle arrival to the nuclear surface.

The particle-particle interactions are executed in the same way as the ones described in the event generator phase. These processes usually have more than one resulting channel. For example, two neutrons can react by the elastic scattering or the inelastic delta particle plus a nucleon formation. The collision probability of two particles depends on their relative position and momentum, the theoretical cross section, and the Pauli exclusion principle. In the case of the induced neutrino reactions, the following interactions are considered: $NN \to NN$, $NN \leftrightarrow NR$, $mN \to R$, $\pi NN \to NN$, and $mN \to mN$, where N represents a nucleon, R represents a baryonic resonance, and m represents a meson. The implemented resonances are Δ_{1232}, Δ_{1950}, Δ_{1700}, Δ_{1950}, N_{1440}, N_{1520}, N_{1680}, and N_{1535}. The mesons are: π, Ω, ρ, and ϕ.

The particle kinematics is implemented in a relativistic way. This is very useful for the calculation of the cross section since it allows determining the 4-momentum of any particle in any desired reference frame. For two particles (or system of particles) of 4-momentum $p = (\epsilon, \mathbf{p})$ and $P = (E, \mathbf{P})$, respectively, in a reference frame K, we can find the momentum p in the reference frame K' at the rest system of P as follows [41]:

$$\mathbf{p}' = \mathbf{p} + \boldsymbol{\beta}\gamma\left(\frac{\gamma}{\gamma+1}\boldsymbol{\beta}\mathbf{p} - \epsilon\right), \tag{3}$$

$$\epsilon' = \gamma(\epsilon - \mathbf{p}\boldsymbol{\beta}), \tag{4}$$

where $\boldsymbol{\beta} = \mathbf{P}/E$, $\gamma = E/M$ and $P^2 = M^2$. The inverse transformation is obtained by substituting $\boldsymbol{\beta} = -\boldsymbol{\beta}$.

A particle can decay when its mean lifetime is lower than the cascade duration time. The decaying time is randomized using the probability density function (PDF)

$$f(t) = 1 - e^{-\lambda t}, \tag{5}$$

where λ is the decay constant. The branching fractions and λ values for all decaying particles were taken from Ref. [42].

Finally, when a particle reaches the nuclear surface, if its kinetic energy is higher than the potential well, it is ejected from the nucleus. Otherwise, the particle is reflected and continues its motion inside the nucleus. Coulomb's potential barrier and the tunnel effect are considered for charged particles.

The intranuclear cascade ends when there are no particles with enough kinetic energy to escape from the nucleus and there are no mesons or baryonic resonances inside the nucleus. Up to this stage, the CRISP provides the following information: type, energy, and momentum of the emitted particles and the mass number A, charge Z, momentum P, angular momentum L, and excitation energy E^* of the residual nucleus.

C. Evaporation fission

When the intranuclear cascade is finished, no nucleon has enough energy to leave the nucleus, but nuclear excitation energy is generally higher than the nucleon binding energy. In this case, excitation energy is redistributed in such a way that particle evaporation could be possible. CRISP simulates the evaporation fission through the Monte Carlo for Evaporation-Fission (MCEF) model [29,38] that has the following characteristics:

(i) The nucleus is in thermodynamic equilibrium.
(ii) It is considered evaporation of protons, neutrons, and alpha particles.
(iii) The evaporation probability is calculated with Weisskopf's statistical model [43].
(iv) The fission probability is calculated through the theory of Vandenbosch and Huizenga [44].

As initial data, we have A, Z, and E^*. In each iteration, the probability of neutron, proton, alpha emission, and nuclear fission are determined. These probabilities are used to aleatory select the event of the iteration. The evaporation-fission model runs as long as the excitation energy is higher than the minimum of the neutron binding energy B_n and the fission energy B_f. If the fission occurs, then the simulation is stopped, and the calculation of the fission fragments is started. When a particle is emitted, A, Z, and E^* are updated to pass to the next iteration.

D. Comparison with other event generators

Next, we examine the main similarities and differences between CRISP and other event generators, such as NUANCE [45], NuWro [46], and GiBUU [47]. These models consider that the nucleus target is a Fermi gas, where the nucleons have been subjected to the Fermi movement and Pauli blocking principle. After the first neutrino–nucleon interaction, the intranuclear cascade begins, executing all the possible interactions between the hadrons inside the nuclear system.

NUANCE is the official Monte Carlo event generator used by the MiniBooNE experiment. In NUANCE, the nucleus is built as a Smith-Moniz relativistic Fermi gas model [48]. The initial momentum of the nucleons is distributed uniformly between 0 and P_F, where P_F is the Fermi momentum. To consider the Pauli blocking, scattering is only allowed when the resulting nucleon has a momentum higher than P_F. If this condition was not applied, nucleons would interact between them and spontaneously evaporate from the nucleus. NUANCE uses a free parameter κ to scale the nucleon lower bound energy E_{lo} and reproduces the CCQE neutrino muon $\frac{d\sigma}{dQ^2}$ on ^{12}C. E_{lo} is defined as the lowest energy of an initial nucleon that leads to a final nucleon just above the Fermi energy level. The pion–nucleon interaction is also tuned to reproduce the $\pi + {}^{12}$C absorption data.

NuWro, in addition to a local Fermi gas model, uses the spectral function's formalism, which determines the probability density functions for the energy and momentum of bound nucleons. This approach, combined with the impulse approximation [49], was necessary to reproduce the Quasielastic (QE) electron-nucleus data. In NuWro, spectral functions are used to describe only the QE interactions, which leads to consider two different ground states: one for the QE interaction and the other for the remaining interactions [50].

Neither NUANCE nor NuWro considers any binding potentials, and the binding energy is introduced as a correction to the final energy spectrum of the emitted particles. In these generators, only the nucleons ejected from the Fermi sea are spatially propagated [50].

Among the event generators studied, GiBUU offers the most realistic description of the neutrino-nucleus reaction. It solves Boltzmann-Uehling-Uhlenbeck (BUU) transport equations numerically [51]. These equations determine the time evolution of the distribution functions for each particle $f_1(\mathbf{r},\mathbf{p},t)$. To calculate $f_1(\mathbf{r},\mathbf{p},t)$, GiBUU considers both nuclear and Coulomb potentials. The use of a nuclear potential allows us to treat the nucleus as a system of bind nucleons. GiBUU uses the nucleon bind energy $B = 8$ MeV [50]. The Pauli blocking is implemented in a stochastic form, since the probability that a reaction $1 + 2 \to 3 + 4$ is forbidden depends on the distribution functions $f_1^1(\mathbf{r},\mathbf{p},t)$ and $f_1^2(\mathbf{r},\mathbf{p},t)$ of the initial particles [52]. The nucleus is constructed under a local RFG model.

III. NEUTRINO-NUCLEON INTERACTION MODEL

The neutrino-nucleon interaction is described through electroweak interactions in the Standard Model framework. It can be represented by Fig. 1.

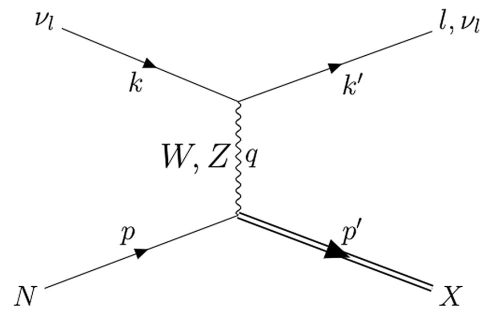

FIG. 1. Neutrino-nucleon interaction.

The neutrino ν_l (antineutrino $\bar{\nu}_l$) with momentum k interacts with the nucleon N with momentum p by a boson exchange with a momentum transferred q. The resulting particles are the lepton (momentum k') and the baryon or another hadronic system X (momentum p'). The contribution of the lepton vertex to the cross section can be calculated in exact form since the neutrino (antineutrino) and the corresponding lepton are elementary particles and the coupling of this interaction is well known from the electroweak formalism.

The hadronic vertex contribution (nucleon-boson-hadronic system) depends on the neutrino interaction with the entire nucleon or with its quark constituents. Therefore, the type of the neutrino-nucleon interaction is determined by the hadronic vertex, which depends essentially on the neutrino energy. In the following, the implemented neutrino-nucleon channels will be described. In general, the equations depend on the square of the momentum transferred denoted as $Q^2 = -q^2$ and given by

$$Q^2 = 2E_\nu E_l - 2|\vec{k}||\vec{k'}|\cos\theta - m_l^2 \tag{6}$$

and

$$W^2 = M^2 + 2M(E_\nu - E_l) - Q^2, \tag{7}$$

where E_ν is the neutrino energy, θ is the emission angle of the lepton l with respect to the direction of the neutrino, M is the mass of the nucleon, m_l is the mass of the lepton, and W is the invariant mass of the hadronic system produced.

A. Quasielastic channel

In the CC, the neutrino and the nucleon interact by a boson W exchange, producing a nucleon and the neutrino corresponding lepton. The cross section for this process is given by Ref. [52]

$$\frac{d\sigma^{\nu,\bar{\nu}}}{dQ^2} = \frac{M^2 G_F^2 \cos^2\theta_C}{8\pi E_\nu^2}\left[A \mp \frac{s-u}{M^2}B + \frac{(s-u)^2}{M^4}C\right], \tag{8}$$

where the negative sign of B is for neutrinos and the positive sign is for antineutrinos. In the previous equation, s and u are the Mandelstam variables. The A, B, and C parameters depend on the vector $F^V_{1,2}(Q^2)$, axial $F_A(Q^2)$, and pseudoscalar $F_P(Q^2)$ form factors.

In the NC, the neutrino and the nucleon are elastically scattered after the boson Z exchange. In this case, the cross section is [52]

$$\frac{d\sigma^{\nu,\bar{\nu}}}{dQ^2} = \frac{M^2 G_F^2}{8\pi E_\nu^2}\left[A \mp \frac{s-u}{M^2}B + \frac{(s-u)^2}{M^4}C\right], \tag{9}$$

Now, the A, B, and C parameters depend on the vector $\tilde{F}^N_{1,2}(Q^2)$, axial $\tilde{F}^N_A(Q^2)$ and strange $F^S_{1,2,A}(Q^2)$ form factors. The superscript N represents the neutron or proton form factor.

In this work, we will discuss the influence of different parametrizations of the F_A, F^S_1, F^S_2, and F^S_A form factors,

$$F_A(Q^2) = \frac{g_A}{(1+\frac{Q^2}{M_A^2})^2} \tag{10}$$

$$F^S_1(Q^2) = -\frac{F^S_1(0)Q^2}{(1+\tau)(1+\frac{Q^2}{M_V^2})^2}, \tag{11}$$

$$F^S_2(Q^2) = \frac{F^S_2(0)}{(1+\tau)(1+\frac{Q^2}{M_V^2})^2}, \quad \text{and} \tag{12}$$

$$F^S_A(Q^2) = \frac{\Delta s}{(1+\frac{Q^2}{M_A^2})^2}, \tag{13}$$

where $g_A = -1.267$, $M_V = 0.843$ GeV, and $\tau = \frac{Q^2}{4M^2}$. The deduction and other form factor expressions for the previous expressions can be found in Refs. [1,52,53].

B. Baryonic resonance formation

In the CC, the neutrino and the nucleon interact by boson W exchange, producing a baryonic resonance and the neutrino corresponding lepton. In the NC, the neutrino is scattered with the nucleon by the boson Z, producing a baryonic resonance.

1. $\Delta(1232)$ resonance

In this case, a different expression is needed for the hadronic current (regarding the quasielastic case) and thus a different relation between the form factors and the hadronic tensor. In fact, for the Δ^{++}, one has [54]

$$\frac{d\sigma^2}{dQ^2dW} = \frac{G_F^2}{4\pi}\cos^2\theta_C \frac{W}{ME_\nu^2}\left\{W_1(Q^2+m_\mu^2) + \frac{W_2}{M^2}[2(k\cdot p)(k'\cdot p) - \frac{1}{2}M^2(Q^2+m_\mu^2)] - \frac{W_3}{M^2}\left[Q^2 k\cdot p - \frac{1}{2}q\cdot p(Q^2+m_\mu^2)\right] + \frac{W_4}{M^2}m_\mu^2\frac{(Q^2+m_\mu^2)}{2} - 2\frac{W_5}{M^2}m_\mu^2(k\cdot p)\right\}, \tag{14}$$

where

$$W_i = \frac{f_i(Q^2,E_\nu)}{M\pi}\frac{M_R\Gamma_R}{(W^2-M_R^2)^2+M_R^2\Gamma_R^2}, \tag{15}$$

and the functions f_i depend on the form factors $C_i^{V,A}$. The parametrization of these form factors and their relation with f_i are based on Ref. [54], with $C_5^A(Q^2)$ parametrized according to the relation (2.12) of Ref. [54]. M_R^2 is the central mass resonance.

To obtain the NC cross section from the CC expression, it is necessary to multiply the transition vector form factors of the CC channel by the factor $(1-2\sin^2\theta_W)$ and use the same transition axial form factors. In addition, the emitted muon must be substituted by a neutrino, which means taking $m_\mu = 0$ in Eq. (14) and dropping the factor $\cos\theta_C$, making it 1. For the other $\Delta(1232)$ resonances, the following relationships were used [54,55]:

$$\begin{aligned}
\sigma(\nu_\mu p \to \mu^-\Delta^{++}) &= 3\sigma(\nu_\mu n \to \mu^-\Delta^+)\\
\sigma(\bar{\nu}_\mu n \to \mu^+\Delta^-) &= 3\sigma(\bar{\nu}_\mu p \to \mu^+\Delta^0)\\
\sigma(\nu_\mu p \to \nu_\mu\Delta^+) &= \sigma(\nu_\mu n \to \nu_\mu\Delta^0)\\
\sigma(\bar{\nu}_\mu p \to \bar{\nu}_\mu\Delta^+) &= \sigma(\bar{\nu}_\mu n \to \bar{\nu}_\mu\Delta^0).
\end{aligned} \tag{16}$$

To calculate $\sigma(\bar{\nu}_\mu n \to \mu^+\Delta^-)$ and $\sigma(\nu_\mu p \to \nu_\mu\Delta^+)$, the sign of W_3 must be changed in Eq. (14).

2. Rein and Sehgal formalism

The Rein and Sehgal formalism allows the cross section calculation of the resonant channel for all resonances of mass $1 < W < 2$ GeV. The cross section is given by [56]

$$\frac{d^2\sigma}{dQ^2dW^2} = \frac{G_F^2\cos^2\theta_C Q^2}{2\pi^2 M|\vec{q}^2|}(\Sigma_{++}+\Sigma_{--}), \tag{17}$$

with

$$\Sigma_{\lambda\lambda'} = \sum_{i=L,R,S} c_i^{\lambda} c_i^{\lambda'} \sigma_i^{\lambda\lambda'}, \tag{18}$$

where $\vec{q}$ is the 3D-vector part of the 4-momentum Q, λ and λ' are the helicity of the incident and outgoing leptons, respectively. Coefficients c_i^{λ} depend on the components of the leptonic current j_μ^* in the frame where the resonance is in rest.

$$\begin{aligned} c_L^{\lambda} &= \frac{K}{\sqrt{2}}(j_x^* + i j_y^*) \\ c_R^{\lambda} &= -\frac{K}{\sqrt{2}}(j_x^* - i j_y^*) \\ c_S^{\lambda} &= K\sqrt{|(j_o^*)^2 - (j_z^*)^2|}. \end{aligned} \tag{19}$$

The leptonic current is expressed as a function of λ, λ', Q^2, E_ν, E_l, and $\cos\theta$ in Ref. [56]. The factor K in Eq. (19) is given by

$$K = \frac{|\vec{q}|}{E_\nu\sqrt{2Q^2}}. \tag{20}$$

The partial $\sigma_i^{\lambda\lambda'}$ are calculated as

$$\sigma_{L,R}^{\lambda\lambda'}(q^2, W) = \frac{\pi W}{W^2 - M^2}\sum_{j_z}|\langle R, j_z|F_{\mp}^{\lambda\lambda'}|N, j_z \pm 1\rangle|^2 \times \delta(W - W_0) \tag{21}$$

and

$$\sigma_S^{\lambda\lambda'}(q^2, W) = \frac{\pi W}{W^2 - M^2}\left(\frac{Q^2}{-q^2}\right)\frac{M^2}{W^2} \times \sum_{j_z}|\langle R, j_z|F_0^{\lambda\lambda'}|N, j_z\rangle|^2 \delta(W - W_0). \tag{22}$$

To obtain the operators $F_{\pm,0}^{\lambda\lambda'}$, the Feynman-Kislinger-Ravndal relativistic model is used [57,58]. In this model, the baryon is considered a coupled harmonic oscillator of three quarks. The baryon states $|N, j_z\rangle$ and $|R, j_z\rangle$ are calculated as a combination of states of spin, isotopic spin and orbital excitation mixed symmetries such that the resulting state is symmetric (color symmetry is not considered). The sum is over all the resonance spin z components j_z. The operators $F_{\pm,0}^{\lambda\lambda'}$ are obtained depending on the proposed couplings for the vector current and the vector-axial current of the considered oscillator Hamiltonian. The $\delta(W - W_0)$ function is replaced by a Breit-Wigner distribution. The expressions for all the required elements to obtain the cross section are reported in Ref. [18]. In the implementation of the Rein-Seghal formalism, the $\Delta(1232)$ resonance was not considered, since it was implemented as described in Sec. III B 1.

C. Deep inelastic scattering

The deep inelastic scattering is important for high energies, where the incident neutrino/antineutrino can interact at the quark level with the nucleon and create a corresponding lepton plus a hadronic system X.

The DIS is divided in two steps:

(i) Neutrino-quark interaction and hadronic system X formation. This step determines the interaction cross section. It has a high dependence on nucleon structure through the different structure factors. Kinematically, it depends on the k, k', p and the invariant mass W of the hadronic system (Fig. 1). We used the cutoff mass $W_{\min}^2 = 1.4\ \mathrm{GeV}^2$ [59].

(ii) Hadronization: formation of the constituent hadrons of system X. This process was implemented through the Andreopoulos-Gallagher-Kehayias-Yang hadronization model with the Koba-Nielsen-Olesen scaling law (AGKY-KNO) model described in Ref. [20].

The cross section for this process is [59]

$$\frac{d^2\sigma^{\nu,\bar{\nu}}}{dxdy} = \frac{G_F^2 M E_\nu}{\pi(1 + Q^2/M_{W,Z}^2)^2}\left\{\left(y^2 x + \frac{m_\mu^2 y}{2E_\nu M}\right)F_1 + \left[\left(1 - \frac{m_\mu^2}{4E_\nu^2}\right) - \left(1 + \frac{Mx}{2E_\nu}\right)y\right]F_2 \pm \left[xy\left(1 - \frac{y}{2}\right) - \frac{m_\mu^2 y}{4E_\nu M}\right]F_3 + \frac{m_\mu^2(m_\mu^2 + Q^2)}{4E_\nu^2 M^2 x}F_4 - \frac{m_\mu^2}{E_\nu M}F_5\right\}. \tag{23}$$

In the equation above, $\nu = E_\nu - E_l$ is the energy transferred to the exchange boson, where E_ν is the energy of the incident neutrino and E_l is the energy of the resultant lepton. $Q^2 = -q^2$, $x = \frac{Q^2}{2M\nu}$, and $y = \frac{\nu}{E}$.

In the term containing F_3, the incident neutrino has positive sign, and the antineutrino has negative sign. For the CC, the mass of the boson W is used, and for the NC, the mass of the boson Z is used. The structure functions of the nucleon $F_{2,3}(x, Q^2)$ are expressed relating to the quark distribution functions of the nucleon, $q_i(x, Q^2)$, where $q_i = \{u, \bar{u}, d, \bar{d}\ldots\}$. In this work, the values of the quark distribution functions were taken from Ref. [60]. $F_{1,4,5}$ was determined using the Callan-Gross and the Albright-Jarlskog relations (see Ref. [61]).

D. Coherent pion production

Coherent pion production consists of neutrino interaction with the entire nucleus so that a pion is produced and emitted. When the neutrino reacts with ^{12}C through a neutral current process, we have

$$\nu_\mu(\bar{\nu}_\mu) + {}^{12}\mathrm{C} \to \nu_\mu(\bar{\nu}_\mu) + {}^{12}\mathrm{C} + \pi^0, \tag{24}$$

and when it is through charged current,

$$\nu_\mu(\bar{\nu}_\mu) + {}^{12}\mathrm{C} \to \mu^-(\mu^+) + {}^{12}\mathrm{C} + \pi^+(\pi^-). \tag{25}$$

Using the Berger-Sehgal model [16], the cross section for the NC process is

$$\frac{d\sigma^{NC}}{dQ^2dydt} = \frac{G_F^2 f_{\pi^0}^2}{4\pi^2}\frac{1-y}{y}G_A^2\frac{d\sigma(\pi^0 + {}^{12}\mathrm{C} \to \pi^0 + {}^{12}\mathrm{C})}{dt}, \tag{26}$$

where t is the square 4-momentum exchanged with the nucleus, f_{π^0} is the pion decay constant, and $\frac{d\sigma(\pi^0+{}^{12}\mathrm{C}\to\pi^0+{}^{12}\mathrm{C})}{dt}$ is the $\pi^0 + {}^{12}$C elastic cross section. The axial form factor G_A is

$$G_A = \frac{M_A^2}{Q^2 + M_A^2} \tag{27}$$

with $M_A = 1.0$ GeV.

For the CC process, the following substitutions must be made in Eq. (26): $f_{\pi^0} \to f_{\pi^\pm}$, $\frac{d\sigma(\pi^0+{}^{12}\mathrm{C}\to\pi^0+{}^{12}\mathrm{C})}{dt} \to \frac{d\sigma(\pi^\pm+{}^{12}\mathrm{C}\to\pi^\pm+{}^{12}\mathrm{C})}{dt}$, depending on the charge of the emitted pion. It is also necessary to add a multiplicative factor $C(y, Q^2)$ [16] to account for the muon mass.

The $\pi + {}^{12}$C elastic cross section was parametrized as

$$\frac{d\sigma}{dt} = A_1 \exp^{-b_1 t}, \tag{28}$$

where parameters A_1 and b_1 depend on the kinetic energy of the incident pion. These parameters were taken from Ref. [16].

IV. RESULTS AND DISCUSSION

In the following, the main results obtained for neutrino-nucleus reactions are presented. The experimental data were published by the MiniBooNE experiment [5]. CRISP uses the MiniBooNE ν_μ and $\bar{\nu}_\mu$ flux predictions ($0 < E < 3$ GeV) [62,63] as input data, which is used as the probabilistic density function to generate the incident neutrino energy.

Table I shows the M_A values used in CRISP for neutrino reactions on H and ^{12}C, respectively. The neutrino-H reactions were simulated considering a free proton.

TABLE I. M_A values used in CRISP for H and ^{12}C reactions.

Channel	H (GeV)	^{12}C (GeV)
CCQE	1.026 [39]	1.35 [62]
NCE	1.012 [53]	1.35 [64]
CCRes $\Delta(1232)$	1.05 [54]	1.05 [54]
NCRes $\Delta(1232)$	1.032 [55]	1.032 [53]
Rein and Sehgal Res	0.95 [18]	0.95 [18]
Coherent	⋯	1.00 [16]

A. Charged current quasielastic channel

The CCQE is observed when the neutrino (antineutrino) interacts with a neutron (proton) and produces a negative (positive) muon plus a neutron (proton): $\nu_\mu(\bar{\nu}_\mu) + n(p) = \mu^-(\mu^+) + p(n)$. If T_μ is the muon kinetic energy and θ_μ is its emission angle, then the neutrino energy and the 4-momentum transferred to the neutron can be determined by [62]

$$E_\nu^{QE} = \frac{2m_n' E_\mu - (m_n'^2 + m_\mu^2 - m_p^2)}{2(m_n' - E_\mu + \sqrt{E_\mu^2 - m_\mu^2}\cos\theta_\mu)} \tag{29}$$

and

$$Q_{QE}^2 = -m_\mu^2 + 2E_\nu^{QE}\left(E_\mu - \sqrt{E_\mu^2 - m_\mu^2}\cos\theta_\mu\right), \tag{30}$$

respectively, where $E_\mu = T_\mu + m_\mu$, m_μ is the muon mass, m_p is the proton mass, and m_n' is an effective neutron mass that depends on the carbon bound energy; i.e., we have $m_n' = m_n - E_b$, with $E_b = 34 \pm 9$ MeV. The magnitudes E_ν^{QE} and Q_{QE}^2 were obtained considering the interaction of the neutrino with a nucleon at rest [62]. For that reason, the subscript QE is placed, to differentiate them from the real neutrino energy and 4-momentum transfer.

In Fig. 2, the cross section per neutron for the reaction $\nu_\mu + {}^{12}$C is shown, as a function of the kinetic energy of the incident neutrino. The red line represents the "CCQE-like" cross section when a muon and no pions are emitted. The blue line represents the CCQE cross section, after eliminating the CC1π contribution from the CCQE-like cross section.

The CC1π contribution is defined when the incident neutrino triggers the following sequence of reactions:

$$\begin{array}{ccc} \nu_\mu(\bar{\nu}_\mu) + n(p) & \longrightarrow & \mu^-(\mu^+) + N^* \\ & & \downarrow \\ & & N^* \longrightarrow N + \pi, \end{array} \tag{31}$$

where N^*, N, and π represent a baryon resonance, a nucleon, and a pion, respectively.

The difference between the lines in Fig. 2 is caused by the processes of production and absorption of pions in the

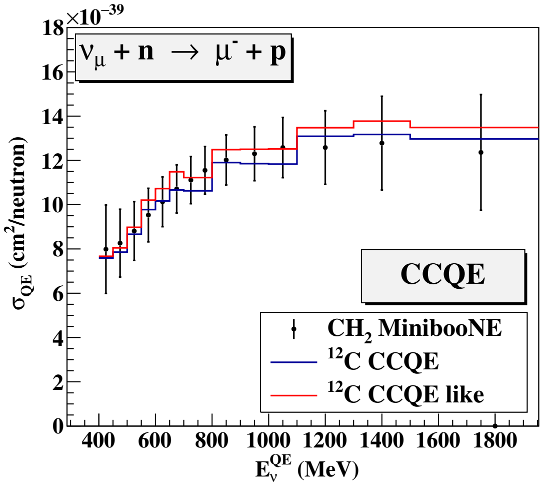

FIG. 2. Total cross section for the reaction $\nu_\mu + n \to \mu^- + p$. The experimental data correspond to the reaction $\nu_\mu + CH_2$ and were taken from Ref. [62]. The simulations were performed for the reaction $\nu_\mu + {}^{12}C$.

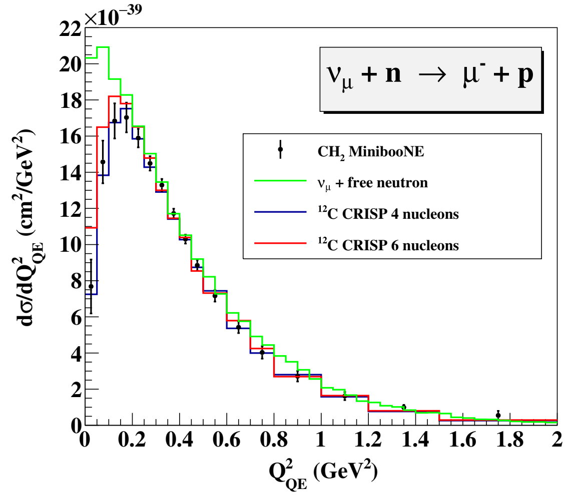

FIG. 3. $d\sigma/dQ^2_{QE}$ cross section per neutron for the channel $\nu_\mu + n \to \mu^- + p$ (CCQE) in reactions $\nu_\mu + {}^{12}C$ (blue and red line) and $\nu_\mu + n$ (green line).

intranuclear cascade. If the pion formed in a CC1π process is absorbed inside the nucleus, then the initial CC1π channel can be detected as a CCQE channel. This CC1π background is considered in the experiment when reporting the CCQE cross section [62]. Figure 2 shows a good agreement between the CRISP simulations and the experimental data.

As explained in Sec. II A, ^{12}C is formed by two energy levels, with occupancy numbers 4 and 12, respectively, and four vacancies in the second level. With this configuration, it is possible to obtain good theoretical-experimental agreement for momentum transfer, except for the region $Q^2 < 0.2$ GeV^2, where CRISP underestimates experimental results (red line in Fig. 3).

It was also considered the model where ^{12}C has no vacancies in the second level, meaning that the maximum number of nucleons in the first two levels are 4 and 8, respectively. This is in agreement with Fermi gas models that are used in other event generators, where the number of vacancies below the Fermi level is always zero. With this configuration, CRISP achieves excellent reproduction of experimental momentum transfer data (blue line in Fig. 3). Thus, all calculations presented in this article use this configuration unless otherwise specified in the text.

Figure 4 shows a comparison between CRISP and NUANCE models. It can be seen that NUANCE needs to use the factor $\kappa = 1.007$ and also multiply the cross section by a factor of 1.08. In CRISP, there is a lower energy limit for bound nucleons in the nucleus. Once the target nucleus is constructed in its ground state, no nucleon can take energy below the lower limit of the first energy level; i.e., the shell model used in CRISP automatically introduces a value of E_{lo}. Thanks to this, it is possible to obtain a good reproduction of the experimental data without readjusting E_{lo}.

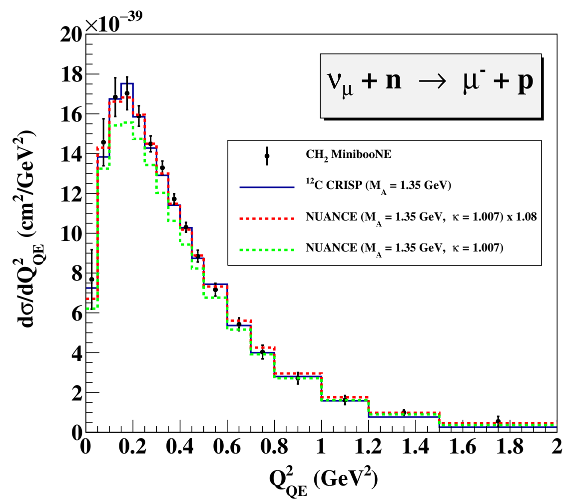

FIG. 4. $d\sigma/dQ^2_{QE}$ cross section per neutron for the channel $\nu_\mu + n \to \mu^- + p$ (CCQE) in reactions $\nu_\mu + {}^{12}C$. The experimental data and NUANCE results were taken from Ref. [62].

Figure 5 shows muon neutrino double-differential cross section for CCQE scattering on hydrocarbon in terms of kinetic energy and scattering angle of the emitted muon. A good agreement between CRISP and the experimental data can be observed. It is important to note that we have made the calculations in ^{12}C, as the two free protons of CH_2 do not interact with the incident muon neutrino through CCQE channel. In Fig. 6, we have the $\frac{d\sigma}{dQ^2}$ cross section for the $\bar{\nu}_\mu + CH_2 \to \mu^+ + n$ reaction (red line) and the $\nu_\mu + {}^{12}C$ reaction (blue line). The red line is calculated as the antineutrino cross section on ^{12}C plus the antineutrino cross section on two free protons. The main difference between the two reactions is in the $0 < Q^2 < 0.2$ GeV^2

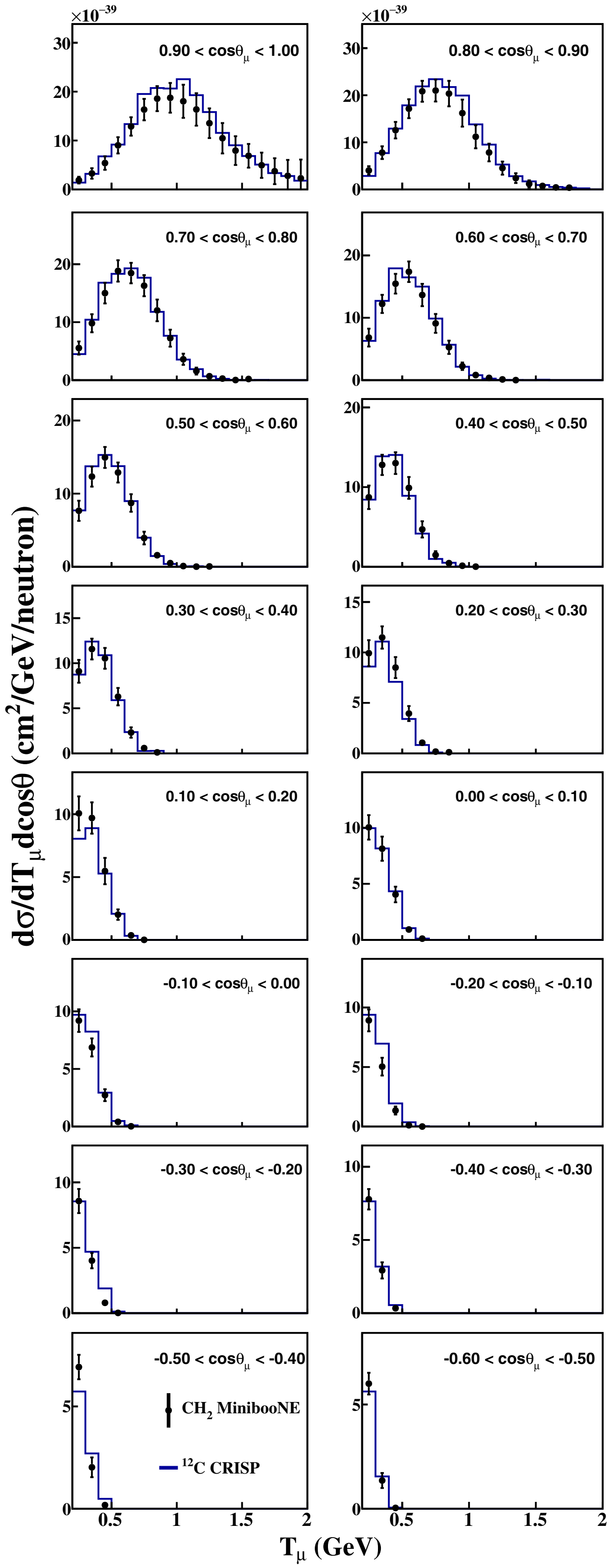

FIG. 5. Double differential cross section $d\sigma/dT_\mu d\cos\theta_\mu$ of emission of μ^- of the CCQE channel. The experimental data were taken from Ref. [62].

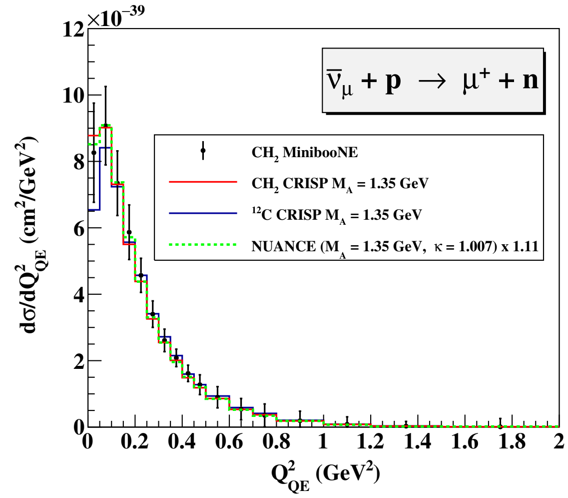

FIG. 6. CCQE $d\sigma/dQ^2_{QE}$ cross section per proton for the reactions $\bar{\nu}_\mu + {}^{12}\mathrm{C}$ (blue line) and $\bar{\nu}_\mu + \mathrm{CH}_2$ (red line). The experimental data and NUANCE results were extracted from Ref. [63].

interval, where the CH_2 cross section is higher than the ^{12}C cross section. That is because the Pauli exclusion principle is not present when the antineutrino interacts with any of the free protons on CH_2. A good agreement of CRISP with the experimental data can be observed in both studied reactions. A comparison between the muon antineutrino double-differential cross section on ^{12}C and free protons is shown in Fig. 7. The cross section on free protons is higher than on ^{12}C for the smallest scattering angles. That is because the Pauli exclusion principle limits the interactions with less energy transfer to the target nucleon and therefore the reactions where the muon spreads forward. In this scattering, the antineutrinos with lower energy transfer less energy to the target nucleon, and there is a higher probability that the Pauli exclusion principle blocks the reaction. For the larger muon scattering angles, it is the opposite, the cross section on ^{12}C is higher than on free protons. In this case, higher energy is transferred to the target nucleon, and therefore Pauli's blocking is less restrictive. Now, the difference between the two reactions is due to the fermionic movement of the nucleons on ^{12}C.

B. Quasi-elastic neutral current channel. Axial and strange form factors

For the measurement of the NCE channel, are selected the events with no muon and no mesons emitted in the intranuclear cascade (NCE-like). According to Ref. [65], the magnitude Q^2 is determined experimentally from the measurement of the total kinetic energy of the emitted nucleons assuming the target nucleon at rest,

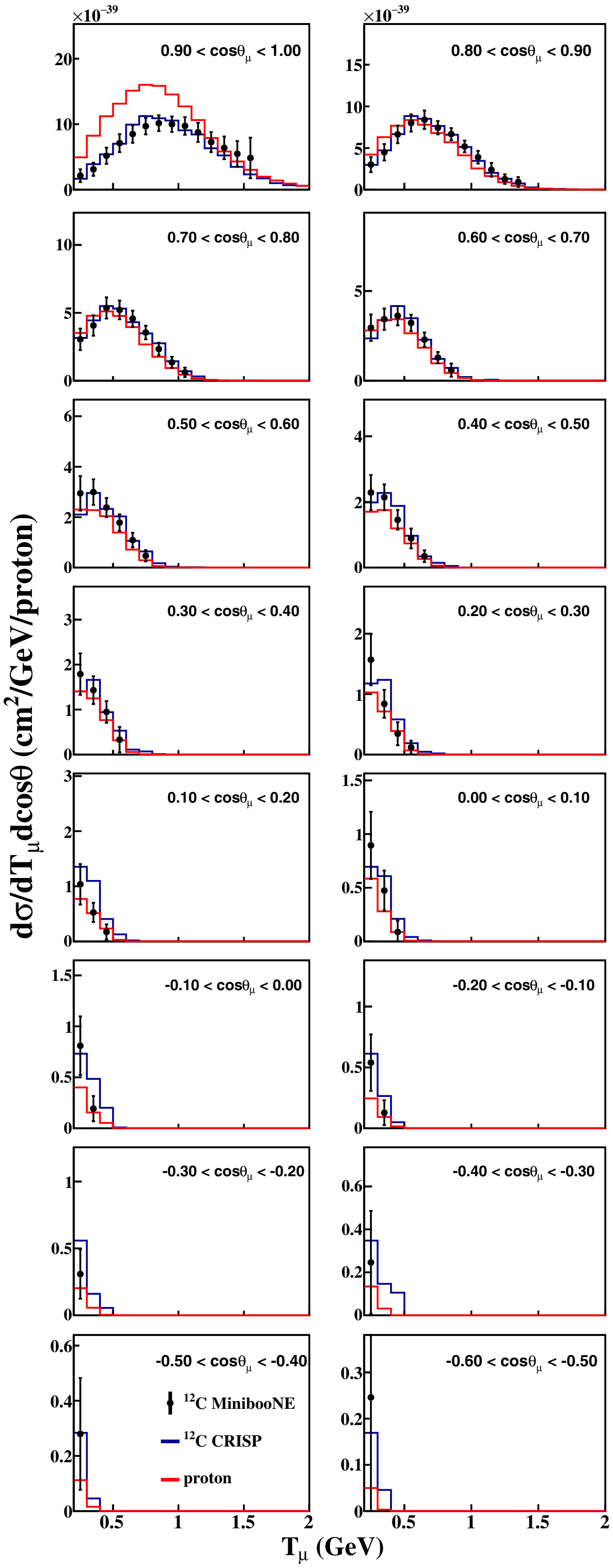

FIG. 7. Double differential cross section $d\sigma/dT_\mu d\cos\theta_\mu$ of emission of μ^+ of the CCQE channel for the reactions $\bar{\nu}_\mu + {}^{12}\mathrm{C}$ (blue line) and $\bar{\nu}_\mu +$ free proton (red line). Experimental data extracted from Ref. [63].

$$Q^2_{QE} = 2m_N T = 2m_N \sum_i T_i, \tag{32}$$

where T is the sum of the kinetic energy T_i of each emitted nucleon.

In addition to the CCQE channel, the following NCE events will be lost and measured as neutral current resonance formation (NCRes):

$$\begin{aligned} \nu_\mu(\bar{\nu}_\mu) + N &\to \nu_\mu(\bar{\nu}_\mu) + N \\ &\swarrow \\ N + N &\longrightarrow N + N^* \\ &\swarrow \\ N^* &\longrightarrow N + \pi. \end{aligned} \tag{33}$$

In addition, the following NCRes channel events will be reported as NCE:

$$\begin{aligned} \nu_\mu(\bar{\nu}_\mu) + N &\to \nu_\mu(\bar{\nu}_\mu) + N^* \\ &\swarrow \\ N^* &\longrightarrow N + \pi \\ &\swarrow \\ \pi + N &\to N + N. \end{aligned} \tag{34}$$

This resonant contribution [Eq. (34)] is considered in the MiniBooNE experiment and taken from the "NCE-like" cross section to obtain the NCE cross section. In Fig. 8, we have the NCE cross section calculated by CRISP for the $\nu_\mu + {}^{12}\mathrm{C}$ (top) and $\bar{\nu}_\mu + {}^{12}\mathrm{C}$ (bottom) reactions.

Since the CRISP code allows knowing the 4-momentum of each involved particle in the reaction, it is possible to calculate the exact value of Q^2 using the formula $Q^2 = -(p'_\nu - p_\nu)^2$, where p_ν and p'_ν are the incident and scattered neutrino 4-momenta, respectively. The $\nu_\mu + \mathrm{CH_2}$ ($\bar{\nu}_\mu + \mathrm{CH_2}$) differential cross section for that calculation is shown in Fig. 9 (red line). It can be observed that the Pauli blocking is relatively less than in the CCQE case, in the region $Q^2 < 0.2\ \mathrm{GeV}^2$ (Figs. 4 and 6). This happens because, in our adopted shell model, nucleons can interact elastically with the incident neutrino in such a way that they fall into the same layer where they were initially located. In the CCQE interaction, when the neutrino interacts with a neutron, for example, the proton formed cannot find vacancies below or in the Fermi layer.

When calculating $d\sigma/dQ^2_{QE}$ using relation (32), we have good agreement between calculation and experiment (blue line, Fig. 9), for $Q^2_{QE} > 0.2\,\mathrm{GeV}^2$. In range $Q^2_{QE} < 0.2\,\mathrm{GeV}^2$, CRISP overestimates the experimental data to the point that it cannot reproduce the peak shape cross section. To explain that, it is necessary to understand how the NUANCE code works [45]. NUANCE is the Monte Carlo simulation model used to process the experimental measurements. It was used to obtain the response matrix during the unfolding process, where it was also considered that there are no systematic

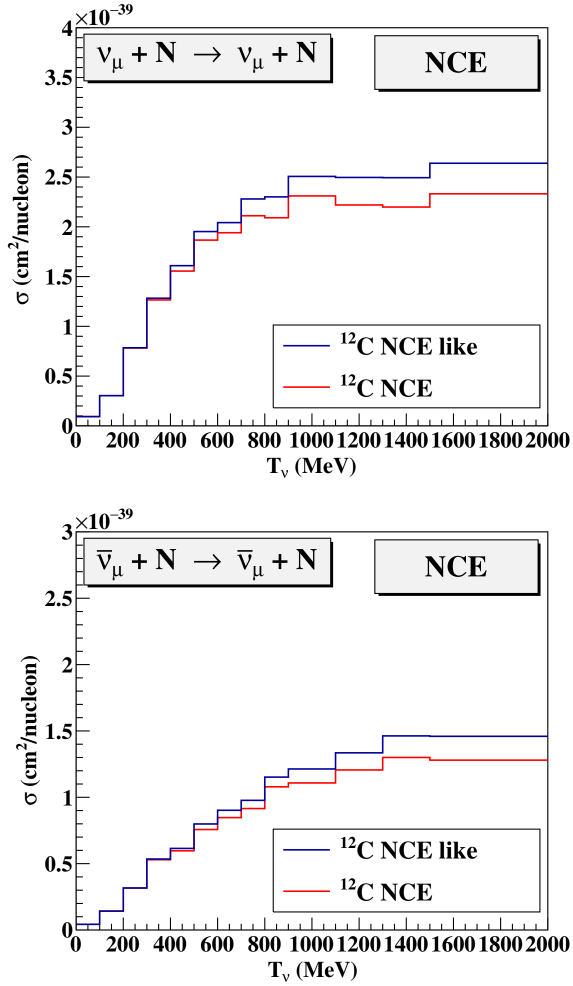

FIG. 8. Cross section per nucleon for the NCE channel for the reactions $\nu_\mu + {}^{12}\text{C}$ (top) and $\bar{\nu}_\mu + {}^{12}\text{C}$ (bottom).

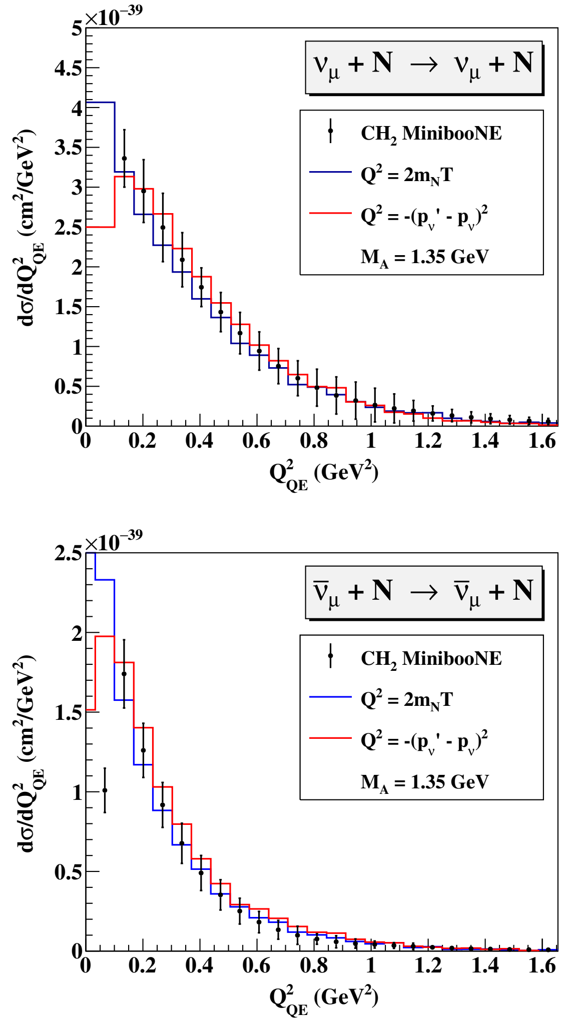

FIG. 9. Top: NCE $d\sigma/dQ^2_{QE}$ cross section per nucleon for $\nu_\mu + \text{CH}_2$ reaction. Bottom: NCE $d\sigma/dQ^2_{QE}$ cross section per nucleon for $\bar{\nu}_\mu + \text{CH}_2$ reaction. Blue line: Q^2_{QE} computed as equation (32). Red line: True Q^2 computed as $Q^2 = -(p_\nu' - p_\nu)^2$ (see the text). Experimental data were taken from Refs. [64,66].

errors in the Monte Carlo predictions [40]. Thus, results obtained in the experiment depend on the NUANCE model.

To understand the importance of modeling the NCE channel, we mention that the experimental method for unfolding the cross section for this reaction involves a delicate Bayesian unfolding method which might result in which Monte Carlo calculations are necessary as a prior distribution [40]. Experimentalists try to reduce the bias by considering different parametrizations of the model embedded in the Monte Carlo calculations. A new model will, of course, further reduce the bias. If we consider that, contrary to the known models, such as NUANCE, where the Pauli blocking is parametrized, in the CRISP model this mechanism is calculated strictly and was tested in many different nuclear reactions, the contribution that the neutrino-nucleus calculations with the CRISP model can give to an improved unfolding of the NCE channel is clear.

In the NUANCE model, to take into account the nuclear effect, the following correction is applied to the cross section [40]:

$$\sigma = (1 - D/N)\sigma_{\text{free}}, \tag{35}$$

where N is the number of nucleons, σ_{free} is the neutrino-free nucleon cross section, and D is

$$D = \begin{cases} \frac{A}{2}\left(1 - \frac{3}{4}\frac{|\vec{q}|}{p_F} + \frac{1}{16}\left(\frac{|\vec{q}|}{p_F}\right)^3\right) & \text{if } |\vec{q}| < 2p_F \\ 0 & \text{if } |\vec{q}| > 2p_F \end{cases}, \tag{36}$$

where A is the mass number, p_F the Fermi momentum, and q the transferred momentum to the target nucleon.

Correction (36) influences the free cross section until where Q^2 represents the emitted nucleons with $T = 90$ MeV, and for that reason, the exclusive carbon neutrino cross section has a peak at $T \approx 90$ MeV (Fig. B.1

from Ref. [40]). In effect, let us consider a valence nucleon with $P = P_F = 220$ MeV$/c$ and a NCE interaction with the maximum transferred momentum so that the cross section is modified by Eq. (36), that is, $q = 2P_F = 440$ MeV$/c$. In that case, the final nucleon momentum can be $P = 440 + 220 = 660$ MeV$/c$. The kinetic energy for that momentum is $T \approx 208$ MeV (inside the nucleus). Considering a nuclear potential of $V = 40$ MeV, the nucleon kinetic energy offside the nucleus is $T \approx 208 - 40 = 168 > 90$ MeV (when it is emitted).

NCE interaction is interesting for the study of axial (F_A) and strange (F_1^S, F_2^S, F_A^S) form factors because, unlike the CCQE channel, we now have a simultaneous contribution of these. Figure 10 (top) shows the $\frac{d\sigma}{dQ^2}$ differential cross section for the $\nu_\mu + CH_2$ reaction and the parametrization of form factors reported in Table II (taken from Ref. [52]). One can observe similar behavior of all parametrizations

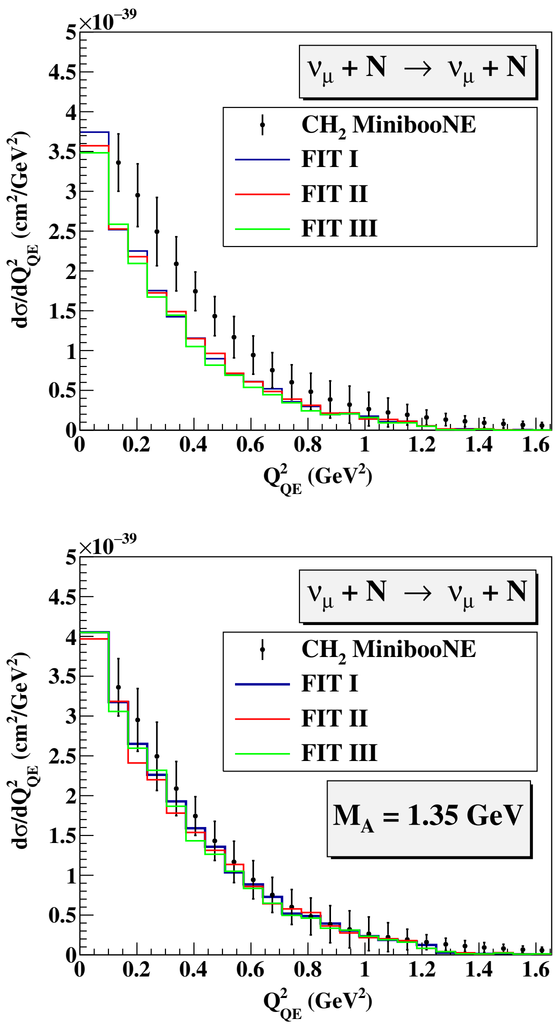

FIG. 10. NCE $d\sigma/dQ^2_{QE}$ cross section for the reaction $\nu_\mu + CH_2$, with parametrization from table II. Top: parameter M_A from Table II. Bottom: parameter $M_A = 1.35$ GeV. Experimental data extracted from Ref. [64].

TABLE II. Parametrization of form factors.

Parameters	FIT I [53]	FIT II [53]	FIT III [52]
Δs	-0.21 ± 0.10	-0.15 ± 0.07	0
$F_1^S(0)$	0.53 ± 0.70	0	0
$F_2^S(0)$	-0.40 ± 0.72	0	0
M_A (GeV)	1.012 ± 0.032	1.049 ± 0.019	1.00

and an underestimation of the experimental data for $Q < 0.7$ GeV^2.

In Fig. 10's bottom panel, we have the same observable as the top panel, this time using the axial mass, $M_A = 1.35$ GeV [65,66]. It is possible to observe a better reproduction of the experimental data. This demonstrates the need to adopt values of M_A for neutrino-nucleus reactions different from those obtained for neutrino-nucleon reactions. Similar results were obtained for the case of the $\bar{\nu}_\mu + CH_2$ reaction (Fig. 11).

C. Neutral current production channel of π^0

The production of neutral current π^0 is measured when there is only one emitted meson (π^0), and there is no muon emission. No restriction is applied to the emission of nucleons [66]. It can be seen how the CRISP model manages to correctly reproduce the shape of the momentum cross section of the emitted pions (12). For the momentum integrated cross section, the $\nu + CH_2$ calculated cross section is $\sigma^{NC\pi^0}_{CRISP} = 4.87 \times 10^{-40}$ cm^2/nucleon, which is in concordance with the experimental result of $\sigma^{NC\pi^0}_{exp} = (4.76 \pm 0.05_{stat} \pm 0.76_{sys}) \times 10^{-40}$ cm^2/nucleon. Similarly, for $\bar{\nu}_\mu + CH_2$ interaction, we have that $\sigma^{NC\pi^0}_{CRISP} = 1.61 \times 10^{-40}$ cm^2/nucleon vs $\sigma^{NC\pi^0}_{exp} = (1.48 \pm 0.05_{stat} \pm 0.23_{sys}) \times 10^{-40}$ cm^2/nucleon.

The superproduction of pions in the interval $0.15 < p^0_\pi < 0.25$ GeV$/c$ may be associated with the fact that the pions are not being absorbed or exchanging charge correctly in the intranuclear cascade. This overproduction is reflected at lower pion emission angles (Fig. 13), where the CRISP angular distribution is more homogenized than the experimental data.

To check how pions interact inside the nucleus, we present a CRISP calculation of the absorption and charge exchange cross sections for the $\pi^\pm + {}^{12}C$ reactions (Fig. 14). The charge exchange cross section is well reproduced by the CRISP code, but on the other hand, CRISP underestimates the pion absorption in the resonant region. This underestimation is higher in the case of negative pions.

D. Charged current production channel of π^+

The production of charged current positive pion ($CC1\pi^+$) is measured when there is only one emitted pion (π^+) and one muon [68]. The most contributing channel to

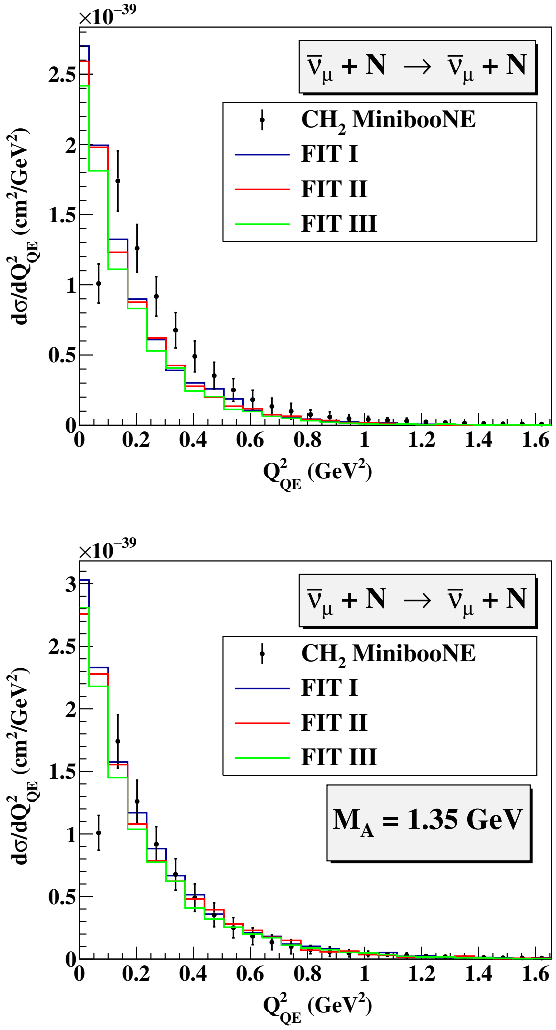

FIG. 11. NCE $d\sigma/dQ^2_{QE}$ cross section for the reaction $\bar{\nu}_\mu + CH_2$, with parametrizations from Table II. Top: parameter M_A from Table II. Bottom: parameter $M_A = 1.35$ GeV. Experimental data extracted from Ref. [66].

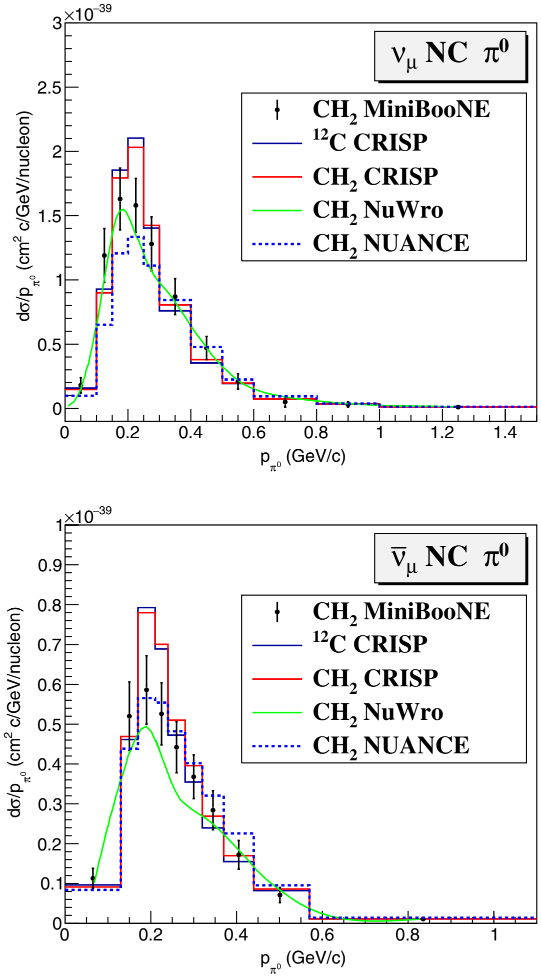

FIG. 12. Linear momentum distribution of emitted NC π^0 during the intranuclear cascade. Experimental data extracted from Ref. [66].

this is the neutrino (antineutrino) resonance formation and the decaying of that resonance:

$$\begin{aligned}\nu_\mu(\bar{\nu}_\mu) + N \to \mu^-(\mu^+) + &N^* \\ &\downarrow \\ &N^* \to N + \pi.\end{aligned} \tag{37}$$

The CCQE interaction can have a contribution to the CC1π^+ channel:

$$\begin{aligned}\nu_\mu(\bar{\nu}_\mu) + n(p) \to \mu^-(\mu^+) + p(n)& \\ \swarrow\quad& \\ p(n) + N \to \quad N + N^*& \\ \swarrow& \\ N^* \to N + \pi.&\end{aligned} \tag{38}$$

CRISP offers a good reproduction of the CC1π^+ emitted μ^- and $\pi+$ kinetic energy distributions, despite the small data underestimation obtained (Fig. 15). In general, other event generators also underestimate this cross section, which shows that the theoretical channels considered are not sufficient to explain a fraction of the emitted CC pions [68,69].

In CRISP, the baryon resonances are propagated inside the nucleus until they decay, depending on their decay channels, which predominantly contain at least one pion. The formation of a resonance through an initial neutrino-nucleon interaction [Eq. (37)] cannot be blocked by Pauli's principle, since this resonance is the first one formed. The unique influence that Pauli's blocking can have on the pion formation through a resonant channel is that some resonance cannot be decay. That occurs if the nucleon resulting from the decay does not find vacancies within the level structure of the nucleus. In this case, the

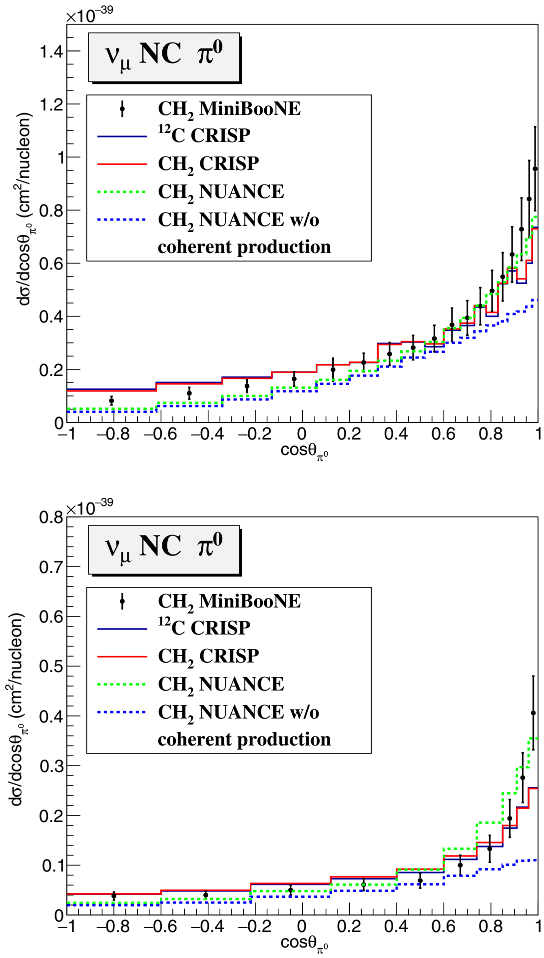

FIG. 13. Angular distribution of emitted NC π^0 during the intranuclear cascade. The emission angle is taken regarding the incident neutrino. Experimental data extracted from Ref. [66].

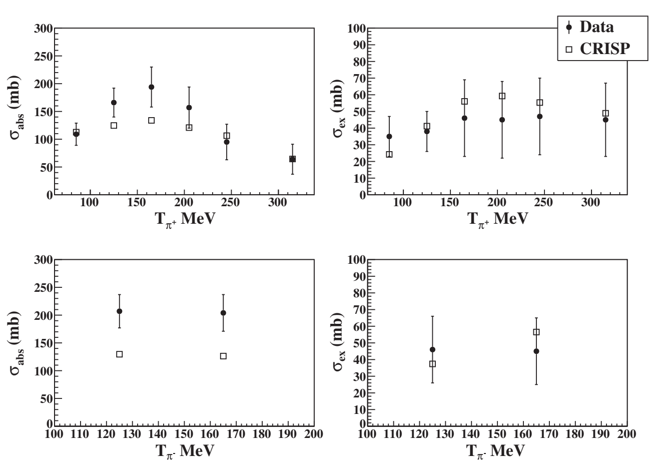

FIG. 14. Absorption cross section σ_{abs} and charge exchange σ_{ex} for $\pi^{\pm}$ in ^{12}C. The absorption cross section is measured when pions are not emitted during the intranuclear cascade. The charge exchange cross section is calculated when only one pion is emitted with charge different from the incident pion. Experimental data extracted from Ref. [67].

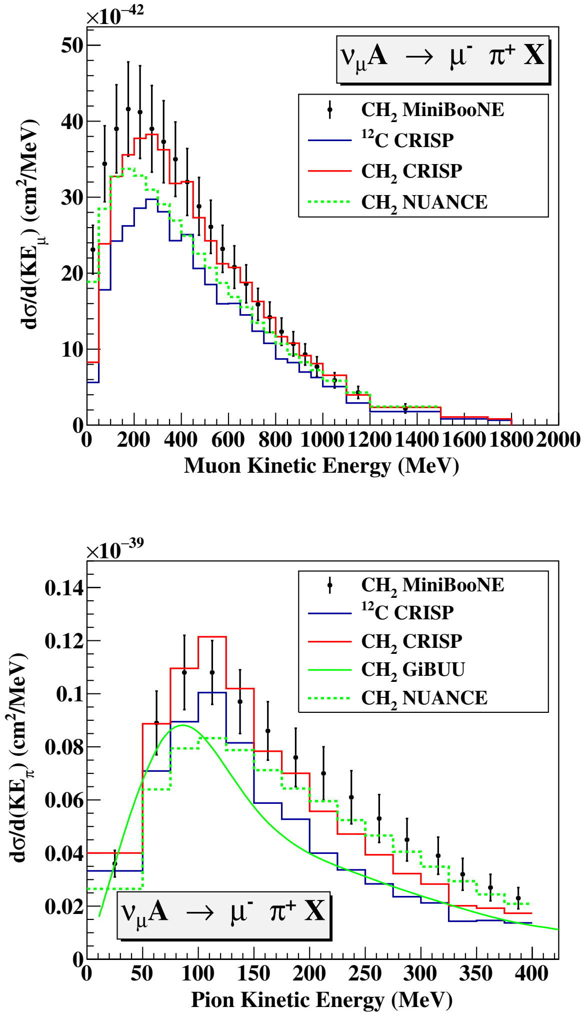

FIG. 15. Kinetic energy distributions of emitted CC μ^- (top) and π^+ (bottom) for the reactions $\nu_\mu + {}^{12}$C and $\nu_\mu + CH_2$. Experimental data and NUANCE calculations were extracted from Ref. [68]. GiBUU calculations were extracted from Ref. [69].

baryonic resonance has to be emitted or absorbed through the $N^* + N \to N + N$ inelastic collision.

E. Three-particle interaction

We start this section with an analysis of the pion-nucleus reaction. Figure 16 shows the experimental nuclear mass number dependence of the exclusive cross section for the π^+-nucleus reaction. If we emphasize the inelastic and absorption channels, we can see a notable difference in the cross section slope. The inelastic channel occurs, in most cases, when the incident π^+ scatters by pion-nucleon collisions inside the target nucleus in such a way that it leaves the nucleus. On the other hand, that π^+ cannot be absorbed through pion-nucleon reactions; it has to be absorbed by at least a couple of nucleons, hence the need to introduce a pion-nucleon-nucleon absorption mechanism to describe the pion-nucleus reaction. In this way, as the

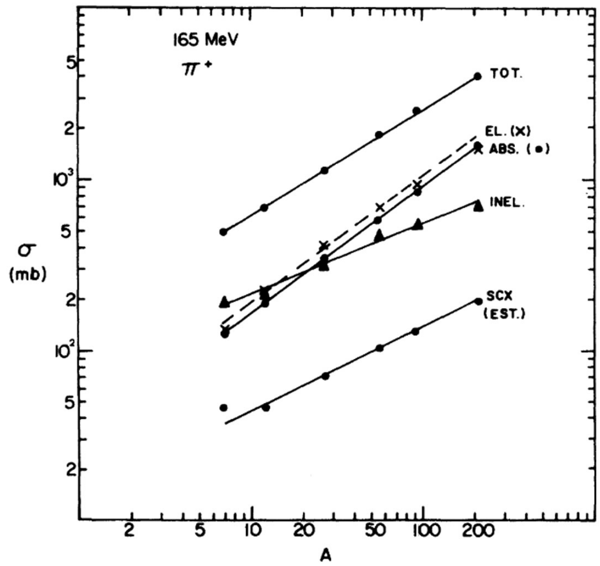

FIG. 16. Decomposition of the total π^+-nucleus cross section at 165 MeV. Figure extracted from Ref. [67].

mass number of the target nucleus increases, the number of possible pairs of nucleons that can absorb the incident π^+ increases more than the number of nucleons that can scatter it, and therefore the absorption channel slope is greater than the inelastic channel slope.

In general, we can establish that the cross section dependence with the target mass number offers relevant information about the primary interaction nature, specifically, if the incident particle interacts with target nucleons independently or with more than one simultaneously. We will apply this methodology and determine if the neutrino-nucleon interaction is sufficient to describe the neutrino nucleus reactions under our intranuclear cascade formalism.

Figure 17 shows the CCQE neutrino-neutron cross section for incident muon neutrinos on deuterium and

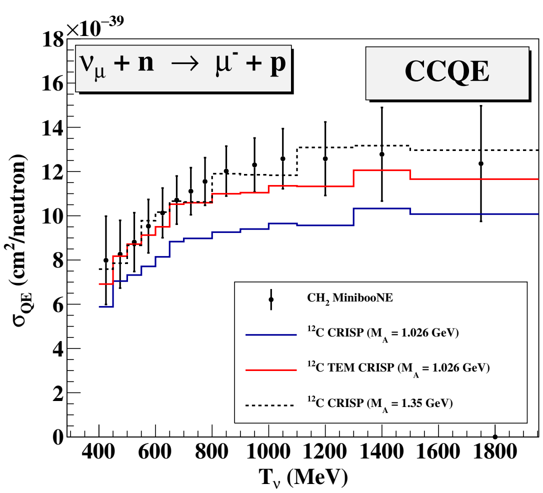

FIG. 17. Experimental (points) and calculated (lines) CCQE neutrino-neutron cross section on deuterium (D_2) and ^{12}C.

^{12}C. The experimental cross section on ^{12}C is higher than on deuterium, but that should not happen since, on ^{12}C, the Pauli blocking mechanism is more effective than on deuterium. For this reason, it is necessary to use a different axial mass parameter M_A in the ^{12}C reaction ($M_A = 1.35$ GeV) than in the neutrino nucleon interaction ($M_A = 1.026$ GeV [39]). In Sec. IV B, we showed that $M_A = 1.012$ GeV does not reproduce the neutrino-^{12}C experimental results.

Figure 20 represents the neutrino nucleus cross section as a function of the number of neutrons on the target nucleus. We selected $E_\nu = 0.6$ GeV because, for that energy, the experimental data reasonably agree with the theoretical predictions (Fig. 17). It can be observed that with the variation of M_A (black and black dashed lines) the linear behavior of σ_{CCQE} does not have a change in the slope, Therefore, we can conclude that under the adopted intranuclear cascade model it will not be possible to reproduce the deuterium and ^{12}C data with the same M_A parameter.

In the case of the CCQE interaction, similar to the pion-nucleon reactions, it is necessary to consider the neutrino interaction with a pair of nucleons (2p2h) to simultaneously reproduce the reactions on D_2 and ^{12}C. Several authors have theoretically investigated this interaction, such as Martini [70,71], Nieves [72,73], and Amaro [74,75]. In this paper, we will use transverse enhancement model (TEM) [76] to test how it works in our multicollisional dynamic.

The transversal enhancement ratio is defined as [76]

$$\mathcal{R}_\tau = \frac{QE_\tau + TE}{QE_\tau}, \tag{39}$$

where QE_τ is the electron-(free nucleon) quasielastic cross section and TE is the transversal enhancement that appears in electron interactions with bound nucleons.

The TEM model parametrizes $\mathcal{R}_\tau(Q^2) = 1 + AQ^2 \exp(-Q^2/B)$, $A = 6\ \mathrm{GeV}^{-2}$, and $B = 0.34\ \mathrm{GeV}^2$. This enhancement is only observed in the transverse response functions, which in the neutrino-nucleon interaction is manifested as a modification of the electromagnetic form factors $G_M^{p,n}$:

$$G_M^{p,n(\mathrm{nuclear})} = G_M^{p,n}(Q^2) \times \sqrt{\mathcal{R}_\tau}. \tag{40}$$

Thus, the cross section exhibits the following transversal enhancement:

$$\frac{d\sigma^{\mathrm{TEM}}}{dQ^2} = \frac{d\sigma^{\mathrm{CCQE}}}{dQ^2}(G_M^{p,n(\mathrm{nuclear})}) - \frac{d\sigma^{\mathrm{CCQE}}}{dQ^2}(G_M^{p,n}). \tag{41}$$

This enhancement is associated with the neutrino interaction with a pair of nucleons (predominantly neutron-proton) interacting through a meson exchange current.

In this work, we will only consider the neutrino interaction with a proton-neutron pair.

Figure 17 shows the CCQE cross section for three different considerations. The dashed black line represents the result obtained earlier in this work for $M_A = 1.35$ GeV. The blue line is the cross section for $M_A = 1.026$ GeV, which is used to describe neutrino deuterium interactions and adopted as the axial mass for the interaction with free nucleons. Both calculations were performed considering only neutrino-nucleon interactions.

With the TEM model (red line), it is possible to reproduce the experimental data, although from 800 MeV onward, an underestimation is observed. In the case of $\frac{d\sigma}{dQ^2}$ for the neutrino and antineutrino reactions (Figs. 18 and 19), the TEM model reproduces the experimental data in interval $0 < Q^2 < 0.5\ \mathrm{GeV}^2$. For larger values, the cross section tends to the same behavior as when only the neutrino-nucleon interaction with $M_A = 1.026$ GeV is considered. This results in an underestimation of the experimental cross section for $Q^2 > 0.5\ \mathrm{GeV}^2$.

The parameters A and B in Eq. (40) were obtained from a fit to the experimental $\mathcal{R}_\tau$ in electron reactions on ^{12}C. This fit underestimates $\mathcal{R}_\tau$ for high values of Q^2, so it is expected to observe this underestimation in neutrino reactions as well. This also explains the underestimation of the total cross section for $E_\nu > 800$ MeV, since the higher the neutrino energy, the higher the contribution of the high Q^2 to the cross section.

In the case of the $\nu_\mu + {}^{12}\mathrm{C}$ reaction, the 2p2h interaction was implemented in CRISP as a correction to the CCQE channel as follows:

(i) A target nucleon satisfying the condition $\sigma^{\mathrm{TEM}}_{\nu-N} > \pi b_{\min}$ is selected (see Sec. II A).

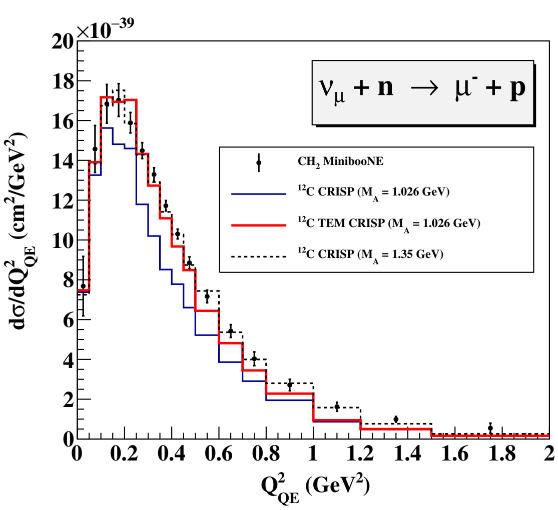

FIG. 18. $d\sigma/dQ^2$ cross section per neutron for the channel $\nu_\mu + n \to \mu^- + p$ (CCQE) in reactions $\nu_\mu + {}^{12}\mathrm{C}$. The experimental data were taken from Ref. [62].

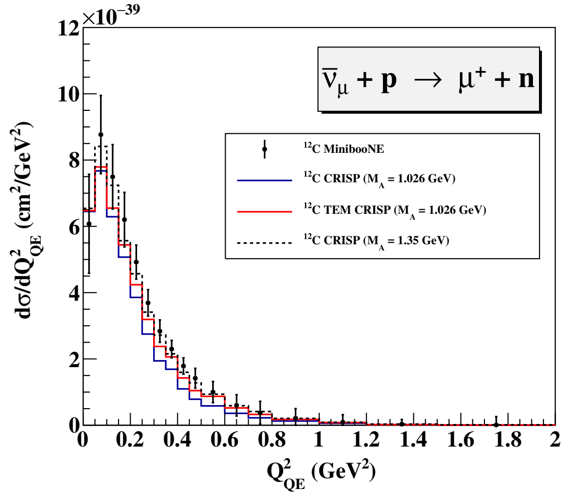

FIG. 19. CCQE $d\sigma/dQ^2$ cross section per proton for the reactions $\bar{\nu}_\mu + {}^{12}\mathrm{C}$. The experimental data and NUANCE results were extracted from Ref. [62].

(ii) The other nucleon of the proton-neutron pair is selected in such a way that the distance to the first nucleon is less than 4.3 fm, which represents the deuterium diameter.

(iii) Once the momentum of the formed muon is determined, the remaining momentum is transferred to the proton-neutron pair.

(iv) The proton and neutron momentum is generated isotropically in the center-of-mass system of the proton-neutron pair [77].

(v) An inverse Lorentz transformation is performed to calculate the momentum of the proton and neutron in the laboratory reference frame of the target nucleus.

We do not consider any correlation between the selected nucleon pairs, except that the distance between them is less than 4.3 fm, to ensure that they have the geometrical possibility to form a quasideuterium pair. We supposed that any other type of correlation is already implicit in the value of the cross section.

This approach allows extending the TEM model for nuclei other than ^{12}C using the CRISP code. For that, it is necessary to estimate the elementary $\nu_\mu + np(\bar{\nu}_\mu + np)$ cross section, which on ^{12}C is $\sigma^{\mathrm{TEM}}_{np} = \sigma^{\mathrm{TEM}}/\langle N_{np}\rangle$, where $\langle N_{np}\rangle$ is the average number of nucleon pairs that can be founded inside a sphere of radius $R = 4.3$ fm. With CRISP, it was determined that $\langle N_{np}\rangle = 5.59$. Then, for nuclei other than ^{12}C, we calculate σ^{TEM} as $\sigma^{\mathrm{TEM}}_{np} \times N_{np}$ for each nucleon in the target, where now N_{np} is the number of nucleon pairs that each nucleon can find at a distance less than 4.3 fm.

Figure 20 (red line) shows how with this approach an increase in the sigma slope line is obtained, just as desired. Therefore, it is possible to simultaneously reproduce the

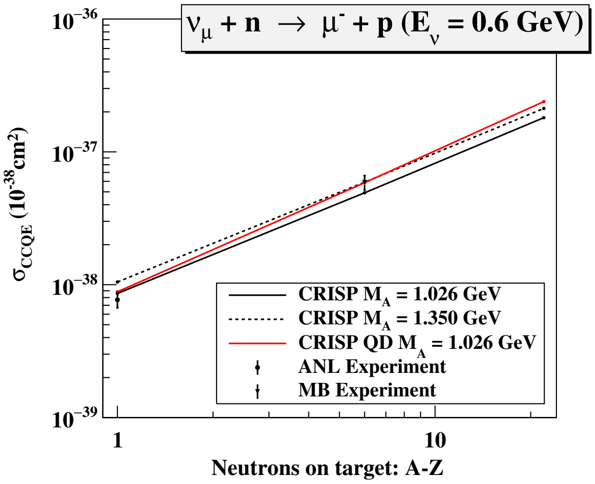

FIG. 20. Dependence of the experimental (points) and calculated (lines) cross section with the target mass number.The black lines are the CRISP calculations under the neutrino-nucleon interactions. The red line represents the CRISP calculations under the neutrino-nucleon and the neutrino-nucleon-nucleon interactions.

experimental neutrino-deuterium and neutrino-^{12}C σ_{CCQE}, both with the same value of $M_A = 1.026$ GeV. To determine if there is a significant neutrino-nucleon-nucleon interaction contribution, measurements on heavier nuclei will be necessary. For example, we present the $\nu_\mu + {}^{40}$Ar reaction, which will be studied soon in the DUNE [12] experiment. Table III shows the σ_{CCQE} predictions for this reaction, according to the form in which the neutrino interacts (with one or two nucleons) and the M_A parameters studied in this work.

Experiments on heavier nuclei are essential for a complete description of the 2p2h interactions, mainly concerning the type of correlation between the nucleons of the proton-neutron pair. It may be the case that the neutrino interacts with the pair as if it were a quasideuterium pair. This interaction was described by Levinger in photon-nucleus reactions, where the photon interacts with the dipole moment of a quasideuterium pair [78]. The cross section is calculated as

$$\sigma = L\frac{NZ}{A}\sigma_{qd}, \tag{42}$$

where $L = 6.4$ is the Levinger factor; N, Z, and A are the neutron, proton, and mass numbers of the target nucleus;

TABLE III. CRISP predictions of the σ_{CCQE} for the $\nu_\mu + {}^{40}$Ar reaction.

M_A (GeV)	$\sigma(10^{-37}$ cm$^2)$	Neutrino interactions
1.026	1.809	$\nu_\mu + N$
1.35	2.123	$\nu_\mu + N$
1.026	2.392	$\nu_\mu + N$, $\nu_\mu + NN$

and σ_{qd} is the cross section for the photon-deuterium reaction.

In the following, we will consider the correlated and uncorrelated cases in the $\nu_\mu + {}^{40}$Ar reaction, which may be interesting to study in the future DUNE experiment. The first step is to estimate σ_{qd}, which can be calculated from the cross section σ_{TEM} on ^{12}C [Eq. (41)] and using the Eq. (42):

$$\sigma_{qd} = \frac{1}{L}\left(\frac{A}{NZ}\right)\Big|_{^{12}\mathrm{C}}\sigma_{\mathrm{TEM}}. \tag{43}$$

In this way, the cross section 2p2h on ^{40}Ar can now be calculated using Eq. (42). From a dynamic point of view, it is necessary to consider the following in CRISP:

(i) The transferred momentum of the incident neutrino is added coherently to the center of mass of the quasideuterium pair.

(ii) Once the momentum of the center of mass of the quasideuterium pair is updated, an inverse Lorentz transformation is performed to calculate the momentum of the proton and neutron in the laboratory reference frame of the target nucleus.

In Fig. 21, top, we calculated the cross section for the reaction $\nu_\mu + (pn) \to \mu^- + pp$ on ^{40}Ar. We used the muon neutrino flux from the MiniBooNE experiment as input data, which is valid for what we want to show. In the figure, it can be seen how the cross section of the uncorrelated case is larger than the correlated one. For the correlated nucleons, the cross section per nucleon is $\sigma/A = L\frac{NZ}{A^2}\sigma_{qd}$, where if we consider $N \approx Z \approx A/2$ we obtain that $\sigma/A \approx 1.6\sigma_{qd}$. According to this, Levinger's formalism is equivalent to a renormalization of the neutrino-nucleon cross section, which is insufficient for obtaining the desired slope in the logarithmic plots of σ vs A (Fig. 20).

The momentum transfer dynamics for the proton-neutron pair occurs differently in the correlated and uncorrelated cases. This could be measured experimentally, for example, by measuring the scattering angle of the emitted protons relative to the direction of the momentum transferred by the neutrino. For a better selection of the 2p2h reactions, cases in which one muon and two protons are emitted could be analyzed. In Fig. 21, bottom, we present the CRISP calculations for this signal, where a remarkable difference between the correlated and uncorrelated cases was also obtained.

The angular distribution of the emitted protons is more directional when the Levinger formalism is applied (Fig. 22). That occurs because the nucleons only gain momentum in the direction of the transferred neutrino momentum. For uncorrelated nucleons, the angular distribution is more homogeneous, since the momentum of the two resulting protons was calculated isotropically in its center-of-mass referential.

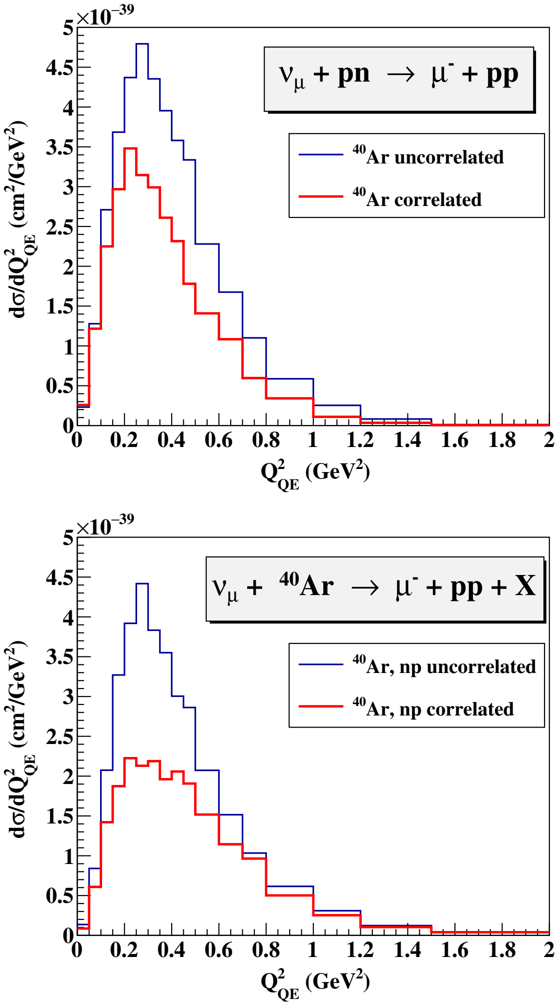

FIG. 21. Top: $d\sigma/dQ^2$ cross section of the 2p2h channel (CCQE) in the reaction $\nu_\mu + {}^{40}\mathrm{Ar}$. Bottom: $d\sigma/dQ^2$ cross section when only one μ^- and two protons are emitted.

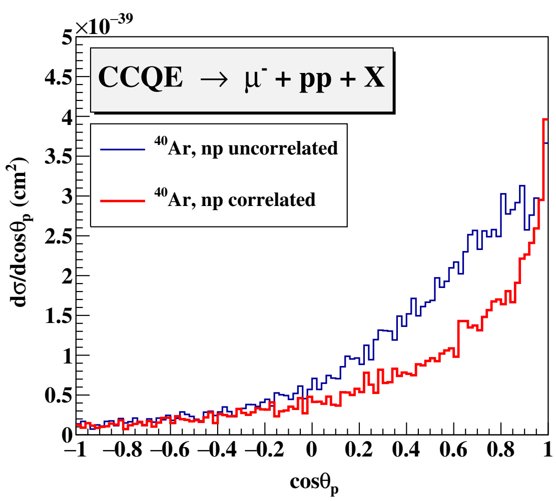

FIG. 22. Proton angular distribution for the reaction $\nu_\mu + {}^{40}\mathrm{Ar} \rightarrow \mu^- + pp + X$.

V. CONCLUSIONS

In this study, the neutrino-nucleus interaction was implemented in the CRISP model. Quasi-elastic channels, baryon resonance production, coherent pion production, and deep inelastic scattering were considered. Comparisons were made with MiniBooNE experimental data and with other event generators, such as NUANCE, NuWro, and GiBUU.

For the CCQE channel, CRISP reproduces the experimental data quite well, using $M_A = 1.35$ GeV, which was the value adopted by NUANCE to perform its simulations. NUANCE employs a RFG model, which allows evaluating whether the introduction of a shell structure offers any improvement in the description of the experimental data. CRISP did not need to use extra parameters or scale the cross section as was done with NUANCE. Thanks to the multicollisional approach and the implementation of an adequate nuclear model, it was possible to observe that the fermionic motion of the nucleons, as well as the Pauli blocking mechanism, have distinctive and appreciable effects both at the momentum transferred distribution and the double differential cross sections.

In the NCE channel, CRISP does not reproduce the experimental cross section for $Q^2_{\mathrm{QE}} < 0.2\ \mathrm{GeV}^2$, especially the peak shape of that curve. Considering the CRISP results and the shape of the neutrino-nucleon cross section, we conclude that this peak should be unreproduced with the use of the RFG model in an intranuclear cascade dynamics. NUANCE reproduces the peak shape but needs to correct the neutrino-nucleon cross section to consider nuclear effects for low Q^2. The results obtained in the MiniBooNE experiment depend on NUANCE since it was used during the unfolding process.

A good reproduction of the NCπ^0 moment distribution was obtained, except for interval $0.15 < p_{\pi^0} < 0.25$ GeV, where CRISP overestimates the experimental data. That may be associated with the fact that CRISP underestimates the pion absorption in the resonant region. The angular distribution presented a more homogeneous behavior to the MiniBooNE data. On the other hand, in the production of CC1π^+, an underestimation of the kinetic energy of emitted π^+ and μ^- is obtained concerning the experimental data. This agrees with that calculated with other generators, such as NUANCE and GiBUU, which shows that the theoretical channels considered are not sufficient to explain a fraction of the emitted π^+.

We also studied the influence of 2p2h processes for the CCQE channel through the TEM model. The importance of these processes lies in the fact that with the adoption of three-particle interaction dynamics it is possible to simultaneously reproduce the experimental data for $\nu_\mu + d_2$ and $\nu_\mu + {}^{12}\mathrm{C}$ reactions with the same axial mass value. The inclusion of the $\nu - NN$ interaction had a notable influence on sigma dependence on the target mass number. As an example calculation, we present our predictions for the

$\nu_\mu + {}^{40}\mathrm{Ar}$ reaction with and without $2p2h$ interactions, which will be measured soon in the DUNE [12] experiment.

The TEM model also allowed us to study the influence of 2p2h reactions on the $\frac{d\sigma}{dQ^2_{QE}}$ cross section. The results obtained with CRISP agree with what was expected for this model: an increase in the cross section relating to the neutrino-nucleon interaction for low Q^2_{QE}. For higher transferred momentum, the TEM cross section tends to the neutrino nucleon cross section, leading to underestimating the experimental cross section in that region.

The study of the 2p2h channel in heavier nuclei may provide information about the correlation between target nucleon pairs. In this work, we evaluated the possibility that the nucleons are uncorrelated, in which situation we applied independent particle dynamics in agreement with the dynamics of the impulse approximation. We also considered the case in which the nucleons are a correlated proton-neutron pair, where Levinger dynamics was applied. Both considerations produce different responses in the 2p2h channel and in reactions where only one muon and two protons are emitted. This study was performed in the $\nu_\mu + {}^{40}\mathrm{Ar}$ reaction, which could be useful for the future DUNE experiment.

ACKNOWLEDGMENTS

Ramon Perez acknowledges the support from CNPq under Grant No. 169813/2017-7. Airton Deppman is supported by the Project INCT-FNA Grant No. 464898/2014-5 and by FAPESP Grant No. 2016/17612-7. Airton Deppman is also partially supported by Conselho Nacional de Desenvolvimento Científico e Tecnológico CNPq (Brazil) under Grant No. 304244/2018-0.

[1] A. W. Thomas and W. Weise, *The Structure of the Nucleon* (Wiley, Germany, 2001).
[2] V. Barger, D. Marfatia, and K. Whisnant, *The Physics of Neutrinos* (Princeton University Press, Princeton, NJ, 2013), pp. 1–224.
[3] J. A. Formaggio and G. P. Zeller, Rev. Mod. Phys. **84**, 1307 (2012).
[4] C. Llewellyn Smith, Phys. Rep. **3**, 261 (1972).
[5] H. Ray, arXiv:hep-ex/0701040.
[6] J. L. Alcaraz-Aunion, AIP Conf. Proc. **967**, 307 (2007).
[7] R. Gran, AIP Conf. Proc. **981**, 256 (2008).
[8] K. Abe (T2K Collaboration), Nucl. Instrum. Methods Phys. Res., Sect. A **659**, 106 (2011).
[9] J. J. Evans, Adv. High Energy Phys. **2013**, 1 (2013).
[10] M. A. Acero*et al.*, Phys. Rev. Lett. **123**, 151803 (2019).
[11] A. R. Back *et al.*, arXiv:1707.08222.
[12] Deep Underground Neutrino Experiment.
[13] F. Di Lodovico, J. Phys. **888**, 012020 (2017).
[14] D. Rein and L. M. Sehgal, Nucl. Phys. **B223**, 29 (1983).
[15] D. Rein and L. Sehgal, Phys. Lett. B **657**, 207 (2007).
[16] C. Berger and L. M. Sehgal, Phys. Rev. D **79**, 053003 (2009).
[17] F. Ravndal, Il Nuovo Cimento A **18**, 385 (1973).
[18] D. Rein and L. M. Sehgal, Ann. Phys. (N.Y.) **133**, 79 (1981).
[19] C. Berger and L. M. Sehgal, Phys. Rev. D **76**, 113004 (2007).
[20] T. Yang, C. Andreopoulos, H. Gallagher, K. Hofmann, and P. Kehayias, Eur. Phys. J. C **63**, 1 (2009).
[21] T. Leitner, L. Alvarez-Ruso, and U. Mosel, Phys. Rev. C **73**, 065502 (2006).
[22] R. P. Feynman and M. Gell-Mann, Phys. Rev. **109**, 193 (1958).
[23] I. S. Towner and J. C. Hardy, Currents and their couplings in the weak sector of the standard model, in *Symmetries and Fundamental Interactions in Nuclei*, edited by Henley Ernest M *et al.* (World Scientific, Singapore, 1995), pp. 183–249.
[24] P. Stoler, Phys. Rep. **226**, 103 (1993).
[25] M. Nowakowski, E. A. Paschos, and J. M. Rodriguez, Eur. J. Phys. **26**, 545 (2005).
[26] S. J. Barish, J. Campbell, G. Charlton, Y. Cho, M. Derrick, R. Engelmann, L. G. Hyman, D. Jankowski, A. Mann, B. Musgrave, P. Schreiner, P. F. Schultz, R. Singer, M. Szczekowski, T. Wangler, H. Yuta, V. E. Barnes, D. D. Carmony, A. F. Garfinkel, and G. M. Radecky, Phys. Rev. D **16**, 3103 (1977).
[27] N. J. Baker, A. M. Cnops, P. L. Connolly, S. A. Kahn, H. G. Kirk, M. J. Murtagh, R. B. Palmer, N. P. Samios, and M. Tanaka, Phys. Rev. D **23**, 2499 (1981).
[28] A. Deppman, S. B. Duarte, G. Silva, O. A. Tavares, S. Anéfalos, J. D. Arruda-Neto, and T. E. Rodrigues, J. Phys. G **30**, 1991 (2004).
[29] A. Deppman, O. A. P. Tavares, S. B. Duarte, J. D. T. Arruda-Neto, M. Gonçalves, V. P. Likhachev, and E. C. de Oliveira, Phys. Rev. C **66**, 067601 (2002).
[30] A. Deppman, G. Silva, S. Anefalos, S. B. Duarte, F. García, F. H. Hisamoto, and O. A. P. Tavares, Phys. Rev. C **73**, 064607 (2006).
[31] V. P. Likhachev, J. Mesa, J. D. Arruda-Neto, B. V. Carlson, W. R. Carvalho, L. C. Chamon, A. Deppman, H. Dias, and M. S. Hussein, Nucl. Phys. **A713**, 24 (2003).
[32] V. P. Likhachev, J. D. T. Arruda-Neto, W. R. Carvalho, A. Deppman, I. G. Evseev, F. Garcia, M. S. Hussein, L. F. R. Macedo, A. Margaryan, J. Mesa, V. O. Nesterenko, O. Rodriguez, S. A. Pashchuk, H. R. Schelin, and M. S. Vaudeluci, Phys. Rev. C **68**, 014615 (2003).
[33] S. A. Pereira, A. Deppman, G. Silva, J. R. Maiorino, A. dos Santos, S. B. Duarte, O. A. P. Tavares, and F. Garcia, Nucl. Sci. Eng. **159**, 102 (2008).

[34] E. Andrade-II, J. C. M. Menezes, S. B. Duarte, F. Garcia, P. C. R. Rossi, O. A. P. Tavares, and A. Deppman, EPJ Web Conf. **21**, 10001 (2012).

[35] M. Abbasi, H. Panjeh, R. Perez, A. Deppman, E. Andrade-II, F. Velasco, and F. Guzman, Eur. Phys. J. Plus **135**, 845 (2020).

[36] R. P. Varona, Simulation of nucleus—nucleus reactions between 30 and 1000 A MeV with the CRISP code, Master's thesis, Universidade de São Paulo, São Paulo, 2018.

[37] D. Vargas, A. R. Samana, F. G. Velasco, O. R. Hoyos, F. Guzmán, J. L. Bernal-Castillo, E. Andrade-II, R. Perez, A. Deppman, C. A. Barbero, and A. E. Mariano, Phys. Rev. C **96**, 054606 (2017).

[38] A. Deppman, O. A. Tavares, S. B. Duarte, J. D. Arruda-Neto, M. Gonćalves, V. P. Likhachev, J. Mesa, E. C. De Oliveira, S. R. De Pina, and O. Rodriguez, Nucl. Instrum. Methods Phys. Res., Sect. B **211**, 15 (2003).

[39] V. Bernard, L. Elouadrhiri, and U.-G. Meißner, J. Phys. G **28**, R1 (2002).

[40] D. Perevalov, Neutrino-nucleus neutral current elastic interactions measurement in MiniBooNE, Technical Reports No. FERMILAB-THESIS–2009-47, No. 970065, University of Alabama, 2009.

[41] R. Hagedorn, *Relativistic kinematics: A guide to the kinematic problems of high-energy physics* (Benjamin, New York, NY, 1963).

[42] M. Tanabashi *et al.* (Particle Data Group), Phys. Rev. D **98**, 030001 (2018).

[43] V. Weisskopf, Phys. Rev. **52**, 295 (1937).

[44] R. Vandenbosch and J. R. J. R. Huizenga, *Nuclear Fission* (Academic Press, New York, 1973), p. 422.

[45] D. Casper, Nucl. Phys. B, Proc. Suppl. **112**, 161 (2002).

[46] C. Juszczak, J. A. Nowak, and J. T. Sobczyk, Nucl. Phys. B, Proc. Suppl. **159**, 211 (2006).

[47] O. Buss, T. Gaitanos, K. Gallmeister, H. van Hees, M. Kaskulov, O. Lalakulich, A. Larionov, T. Leitner, J. Weil, and U. Mosel, Phys. Rep. **512**, 1 (2012).

[48] R. A. Smith and E. J. Moniz, Nucl. Phys. **B43**, 605 (1972).

[49] L. Alvarez-Ruso *et al.*, Prog. Part. Nucl. Phys. **100**, 1 (2018).

[50] U. Mosel, J. Phys. G **46**, 113001 (2019).

[51] M. Effenberger, Eigenschaften von Hadronen in Kernmaterie in einem vereinheitlichten Transportmodell, Ph.D. thesis, Giessen University, 1999.

[52] T. J. Leitner, Neutrino interactions with nucleons and nuclei, Ph.D. thesis, Institut für Theoretische Physik Justus-Liebig-Universität Gießen, 2005.

[53] G. T. Garvey, W. C. Louis, and D. H. White, Phys. Rev. C **48**, 761 (1993).

[54] O. Lalakulich and E. A. Paschos, Phys. Rev. D **71**, 074003 (2005).

[55] T. Leitner, L. Alvarez-Ruso, and U. Mosel, Phys. Rev. C **74**, 065502 (2006).

[56] K. S. Kuzmin, V. V. Lyubushkin, and V. A. Naumov, Mod. Phys. Lett. A **19**, 2815 (2004).

[57] F. Ravndal, A relativistic quark model with harmonic dinamics, Ph.D. thesis, California Institute of Technology, Pasadena, California, 1971.

[58] R. P. Feynman, M. Kislinger, and F. Ravndal, Phys. Rev. D **3**, 2706 (1971).

[59] S. Kretzer and M. H. Reno, Phys. Rev. D **66**, 113007 (2002).

[60] A. Buckley, J. Ferrando, S. Lloyd, K. Nordstrom, B. Page, M. Ruefenacht, M. Schoenherr, and G. Watt, Eur. Phys. J. C **75**, 132 (2015).

[61] E. A. Paschos and J. Y. Yu, Phys. Rev. D **65**, 033002 (2002).

[62] A. A. Aguilar-Arevalo *et al.*, Phys. Rev. D **81**, 092005 (2010).

[63] A. A. Aguilar-Arevalo *et al.*, Phys. Rev. D **88**, 032001 (2013).

[64] T. M. Collaboration, Phys. Rev. D **82**, 092005 (2010).

[65] A. A. Aguilar-Arevalo *et al.* (T. M. Collaboration), Phys. Rev. D **81**, 013005 (2010).

[66] A. A. Aguilar-Arevalo *et al.*, Phys. Rev. D **91**, 012004 (2015).

[67] D. Ashery, I. Navon, G. Azuelos, H. K. Walter, H. J. Pfeiffer, and F. W. Schleptüz, Phys. Rev. C **23**, 2173 (1981).

[68] A. A. Aguilar-Arevalo *et al.*, Phys. Rev. D **83**, 052007 (2011).

[69] U. Mosel and K. Gallmeister, Phys. Rev. C **96**, 015503 (2017).

[70] M. Martini, M. Ericson, G. Chanfray, and J. Marteau, Phys. Rev. C **80**, 065501 (2009).

[71] M. Martini, M. Ericson, and G. Chanfray, Phys. Rev. C **84**, 055502 (2011).

[72] J. Nieves, I. R. Simo, and M. J. VicenteVacas, Phys. Rev. C **83**, 045501 (2011).

[73] J. Nieves, I. Ruiz Simo, and M. Vicente Vacas, Phys. Lett. B **707**, 72 (2012).

[74] J. E. Amaro, M. B. Barbaro, J. A. Caballero, T. W. Donnelly, A. Molinari, and I. Sick, Phys. Rev. C **71**, 015501 (2005).

[75] J. E. Amaro, M. B. Barbaro, J. A. Caballero, T. W. Donnelly, and C. F. Williamson, Phys. Lett. B **696**, 151 (2011).

[76] A. Bodek, H. S. Budd, and M. E. Christy, Eur. Phys. J. C **71**, 1726 (2011).

[77] J. T. Sobczyk, Phys. Rev. C **86**, 015504 (2012).

[78] J. S. Levinger, Phys. Rev. **84**, 43 (1951).